Seasonal heavy precipitation sensitivity to moisture corrections in the western Mediterranean across resolutions

S. Khodayar [a,*], A. Caldas-Alvarez [b]

[a] *Mediterranean Centre for Environmental Studies (CEAM), Valencia, Spain*
[b] *Institute of Meteorology and Climate Research (IMK-TRO), Karlsruhe Institute of Technology (KIT), Karlsruhe, Germany*

A B S T R A C T

The controlling role of atmospheric water vapour for heavy precipitation leading to extreme events has been widely demonstrated, along with the existing gap of adequate moisture observations and the frequent biases present in model simulations concerning this fundamental variable. In this study, we profit from a state-of-the-art dense network of GPS measurements over Europe retrieving a homogenized GPS-derived Zenith Total Delay (GPS-ZTD) data set up to 10 min of temporal resolution, to assess the seasonal sensitivity of convection-related processes and heavy precipitation modelling to atmospheric humidity corrections. For this purpose, we perform nudging experiments with the COSMO-CLM model at two spatial resolutions, 7 km (parameterized convection) and 2.8 km (explicitly resolved convection) covering the autumn period of 2012, when the Special Observation Period (SOP) 1 of the Hydrological Cycle in the Mediterranean Experiment (HyMeX) program took place in the Western Mediterranean, which is our area of interest.

The benefits and disadvantages of GPS-ZTD nudging and resulting moisture corrections are disentangled. The impact on high-resolution parameterized versus convection-permitting simulations is compared. A process-understanding methodology and a local-to-regional approach are used. Our results show a beneficial impact on the seasonal scale at both model grid spacings improving the representation of the chain of processes leading to heavy precipitation, contrary to the non-systematic improvement at the event and sub-event scales. The correction of atmospheric moisture entails a reduction of about 10% in the total column water vapour and corrections on single locations up to 10 mm counteracting the model wet bias across scales. The location, structure, and amount of total precipitation are positively affected. Particularly, the combination of high-resolution atmospheric humidity observations and fine convection-permitting simulations shows great potential for correction of the precipitation daily cycle, key for accurate precipitation modelling. The difference in the density of local and upstream observational networks and the lack of information on the vertical stratification of moisture are identified weaknesses, which could be determinants in obtaining more accurate corrections on seasonal to sub-seasonal scales after assimilation strategies.

1. Introduction

Atmospheric humidity lies at the heart of all key terrestrial atmospheric processes (Sherwood et al., 2010) playing a fundamental role in the water and energy cycles (Randall et al., 2007). The importance of water vapour in regulating climate is without question. This is the dominant greenhouse gas, trapping more of the Earth's heat than any other gaseous constituent of the atmosphere. If water vapour concentrations increase in a warmer world, the added absorption will act to further amplify the initial warming, thus leading to strong positive feedback on climate.

The interrelation between atmospheric humidity and precipitation, particularly convection and extreme precipitation has been widely investigated in the past (e.g., Trenberth et al., 2003; Zhang et al., 2016; Khodayar et al., 2018a). The amount, vertical stratification, and spatial variability of tropospheric water vapour have been pointed out as key for the initiation, development, and intensification of convection, hence subsequent heavy precipitation (Khodayar et al., 2018b). These characteristics affect local and regional conditions that link atmospheric humidity and precipitation such as stability conditions and the

triggering, timing, and location of convection.

Despite its relevance, atmospheric humidity is generally under-sampled and exhibits a complex life cycle and high spatiotemporal variability across scales. Therefore, it is necessary to measure atmospheric moisture over long-term periods as well as at a high temporal resolution to improve our understanding of its effects on precipitation among other related issues. Up to now, our ability to monitor changes in water vapour was limited by the scarcity of observing systems with enough accuracy and longevity to document its global variation. Water vapour is notoriously difficult to measure, and such a capability would be of great value to the climate research community.

The availability of new technologies to monitor changes in atmospheric humidity with improved spatiotemporal accuracy allows progress in the understanding of convective interaction with water vapour, hence towards improved understanding of the mechanisms leading to heavy precipitation. GPS-technology has been successfully used to better the representation of heavy precipitation over flat and complex terrains (Khodayar et al., 2012), to contribute to the understanding of atmospheric processes at high resolution (e.g. Bastin et al., 2005, 2007; Bock et al., 2007; Champollion et al., 2009; Caldas-Álvarez and Khodayar, 2020), and it has been of pivotal importance to define the spatiotemporal evolution of atmospheric moisture conditions leading to heavy precipitation events in the north-WMed on seasonal (Ricard et al., 2012; Khodayar et al., 2018b; Khodayar et al., 2021; Mascitelli et al., 2021) also at sub-seasonal time scales (Caldas-Álvarez and Khodayar, 2020). Moreover, GPS-derived information allowed the assessment of atmospheric moisture biases in model simulations, which are known to be a well-known source of uncertainty in the prediction of HP. Bastin et al. (2019) showed using GPS information that in Europe RCM models tend to overestimate the low values of IWV, and the use of the nudging technique reduces the differences between GPS and simulated IWV. They point out the limitations of the models to represent land surface-atmosphere exchanges affecting the estimation of IWV over most parts of Europe, particularly in summer, as a reason for humidity biases in contrast with the correct simulations of the dependency between IWV and temperature.

Furthermore, the assimilation of GPS information in numerical weather prediction models has demonstrated promising results showing benefits to the forecast quality (Lindskog et al., 2017). Positive impacts on the forecast of synoptic-scale circulations and seasonal precipitation have been reported (Poli et al., 2007), so as for geopotential height and heavy precipitation (e.g., Boniface et al., 2009). However, data assimilation procedures generally imply the assimilation of other types of observations in addition to the GPS information, which renders it difficult to understand the exclusive impact of the GPS information, hence, to gain knowledge about the IWV-precipitation relationship.

A Météo-France AROME NWP system covering the whole WMed was used to perform an extensive reanalysis of the HyMeX-SOP1 period exploiting observations from research instruments deployed during the campaign in addition to the operational observations assimilated in real-time (Fourrié et al., 2019, 2021). Data denial experiments from the reanalysis at a time clearly showed the benefit of assimilating the reprocessed GPS ground-based zenithal total delays. Furthermore, Caldas-Álvarez and Khodayar (2020) and Caldas-Álvarez et al. (2021) pointed out the benefits and limitations of corrections through GPS-ZTD nudging on selected case studies of heavy precipitation during autumn 2012 providing novel insights on the atmospheric moisture-heavy precipitation interactions. Also, clearly showed, through an in-depth analysis, the positive impact of the nudging on, a) correcting the magnitude of atmospheric and water vapour variability, and b) in better regulation of accumulated precipitation, coming the latter much closer to reality though less intense convection and a lower number of triggered cells. However, they also clearly show that this improvement is not enough to overcome the humidity biases at low-tropospheric levels and the associated errors.

The growing use of GPS-derived observations because of their

inexpensive and "all-weather" availability, their increasing number worldwide, and their demonstrated potential to cover observational gaps, make the assessment of their impact on modelling necessary. Moreover, improved knowledge of the IWV-precipitation relationship is needed to better constrain models for a better prediction of heavy precipitation.

So far, the unavailability of long-term, dense, and homogeneous data sets of water vapour measurements on sub-daily timescales and/or the idealized nature of sensitivity experiments, generally on event-based time scales did not allow an in-depth assessment of the impact of atmospheric moisture biases and correspondent realistic correction on the modelling of HP. In this investigation, we profit from the state-of-the-art dense, homogenized GPS data set (Bock et al., 2016) on 10 min temporal resolution covering the whole north-WMed available in the framework of the HyMeX program (Ducrocq et al., 2014; Drobinski et al., 2014) to fulfill this objective.

We examine, through sensitivity experiments, the atmospheric and heavy precipitation modelling response to a realistic high-resolution correction of atmospheric moisture over the north-WMed through the continuous nudging of 10 min temporal resolution GPS-derived information during the autumn period of 2012. The COSMO-CLM regional climate model is used and the results from convective parametrized and convection-permitting simulations are compared. The paper is organized as follows: in section 2 the model and observational datasets are described. Section 3 describes the methodology followed. The main results are discussed in sections 4, 5, and 6. Finally, conclusions are given in section 7.

2. Data sets and model

2.1. Experimental setup

2.1.1. GPS network and IWV/ZTD observations

GPS receivers provide measurements of the Zenith Total Delays (ZTD) of emitted microwave GPS signals useful for meteorological applications. The delay endured by the GPS L1 and L2 band satellite emissions due to their interaction with the terrestrial atmosphere can be estimated and converted to measurements of precipitable water (Bevis et al., 1992; Businger et al., 1996). The HyMeX project provides a high-quality GPS dataset with large coverage over southwestern Europe (orange dots; Fig. 1), post processed by the LAboratoire de Recherche en Géodésie (LAREG) and made available in several averaging periods, 5 min, 1 h and 3 h, (Bock et al., 2016). In this research work, we use the HyMeX ZTD dataset at 10-min temporal resolution for the nudging experiments.

ZTD measurements can be used to derive Integrated Water Vapour (IWV) observations, a measure of the total precipitable water available at the station location. To this end, mean temperature and pressure
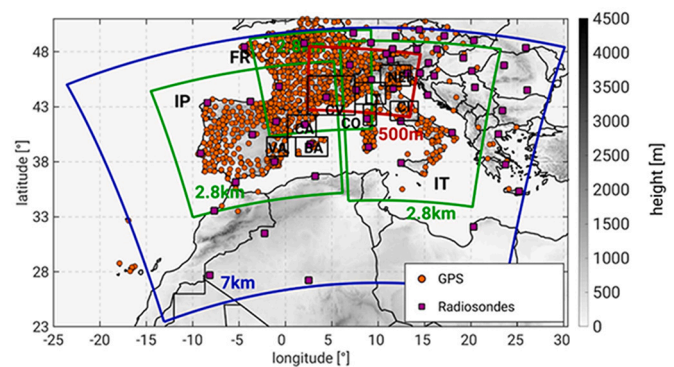

Fig. 1. Area of investigation including simulations domains, climatological subdomains, and target areas (TGA), the position of GPS-ZTD, and radiosondes available during the SOP1 HyMeX campaign.

estimations at the station surface are needed. The HyMeX project provides an IWV product, derived from the original ZTD measurements using ERA-interim mean temperature and pressure (Bock et al., 2016). The HyMeX IWV product is used in this paper for validation of our model results (Figs., 3 and 4).

2.1.2. CMORPH precipitation observations

The Climate Prediction Center (CPC) applies a Morphing technique consisting of propagating microwave satellite precipitation observations using motion vectors derived from geostationary infrared satellites to provide a gridded product with high quality (CMORPH; Joyce et al., 2004). The data set covers the period between 1998 and 2015 and has a temporal frequency of 30 min and a spatial resolution of 8 km. The used microwave retrievals are obtained from the Special Sensor Microwave Imager (SSM/I) aboard the Defense Meteorological Satellites Program 13, 14 & 15, the Advanced Microwave Sounding Unit-B (AMSU-B) on board the National Oceanic and Atmospheric Administration 15, 16, 17 & 18 satellites, the Advanced Microwave Scanning Radiometer-E (AMSR-E) in the Aqua polar-orbiting satellite and the Tropical Rainfall Measuring Mission (TRMM) Microwave Imager (TMI). CMORPH has shown good results in the validation against rain gauges, outperforming other remote sensing products, e.g., the Tropical Rainfall Measurement Mission (TRMM; Jiang et al., 2018), For the investigation period of this study it has been validated against the HyMeX V4 rain gauges (not shown) with an average correlation for the Italy, Spain and France climate regions of 0.7. The data is accessible under request at https://www.ncei.noaa.gov/products/climate-data-records/precipitation-cmorph (last accessed 02-Aug-2021).

2.1.3. Radiosondes

For validation of simulated humidity, we have used operational radiosondes from the HyMeX network (Fig. 1). This data set spans the period between 1997 and 2017 and includes the Special Observation Period 1 (SOP1). The soundings contain up to 30 parameters, such as geopotential height, temperature, dew point temperature, or wind. The temporal resolution ranges between 6 h and 24 h depending on the launching times of the considered station with a vertical resolution of ca. 30 levels. In this paper, we employ all available soundings at three selected stations in the period 01-Sep to 21-Nov. The three selected stations, Barcelona (eastern Spain), Nimes (southern France), and Pratica di Mare (mid, Italy) are chosen due to their low altitude to avoid large height differences between the model's surface and the station. Large surface differences are known to introduce relevant deviations in humidity measurements (Parracho et al., 2018). More information on the data set can be found in Caldas-Álvarez and Khodayar (2020), and Caldas-Álvarez et al. (2021). The data are accessible after registration at http://mistrals.sedoo.fr/?editDatsId=595&datsId= 595&project_name = HyMeX (last access: 3 August 2021). [AC1].

2.2. COSMO-CLM model and the Nudging procedure for GPS-ZTDs

COSMO-CLM is the climate version of the COnsortium for Small-scale MOdelling (COSMO) model. It is based on the non-hydrostatic, thermo-hydrodynamical equations in a limited area approach (Schättler et al., 2009) considering the wind components, temperature, pressure perturbation, the cloud water content, and the specific humidity as prognostic variables (Schättler et al., 2009). The model uses an Arakawa C grid type with terrain-following coordinates and is appropriate for simulations in the meso-α and meso-β scales. Being a climate model, a re-formulation for the slow-changing variables (Ozone and aerosol concentration, canopy variables) is included to account for their seasonal and climate variability, as opposed to the Numerical Weather Prediction (NWP) version. The subgrid-scale turbulence is parameterized using a Turbulent Kinetic Energy (TKE) scheme with a 1D diagnostic closure (Doms et al., 2011). The surface layer parameterization includes a laminar-turbulent roughness layer and a drag-law

formulation for the fluxes (Louis, 1979). The grid-scale clouds and precipitation use a bulk scheme continuity model including water vapour, cloud water, cloud ice, rain snow, and graupel as water species. Moist convection is parameterized using the Tiedtke scheme (Tiedtke, 1989). For model horizontal scales finer than ~3 km only the shallow convection scheme is active. The radiation scheme follows the Ritter and Geleyn (1992). The soil model is the TERRA Multi-Layer (ML) model, based upon the two-layer scheme from Jacobsen and Heise (1982) using 8 soil model levels. The surface data is obtained from the GLOBE dataset (Hastings and Dunbar, 1999) with a 1 km resolution.

The scheme used for assimilation is Nudging or "Newtonian relaxation" (Schraff and Hess, 2012). Provided we assimilate GPS-ZTD measurements (see Sect. 2.1.1) and the fact that the Nudging scheme, as implemented in COSMO-CLM, only allows for the assimilation of prognostic variables, the ZTD measurements need to be converted to specific humidity profiles for all model levels. We feed ZTD observations with a 10-min temporal resolution to the model, within the -1 h, +3 h interval with respect to the observation time stamp. The observations are then assigned to a grid point. COSMO-CLM converts the ZTDs to IWV estimations using simulated mean temperature and pressure at the surface. Afterward, COSMO-CLM builds up a specific humidity profile for each IWV observation. This is done using an iterative method departing from the simulated profile of specific humidity ($q_{v_i}^{mod}$), i.e., first guess (Eq. 1). For every iteration i, the precipitable water of the model (IWV_i^{mod}) is scaled to that of the observations (IWV^{obs}), to increment/decrease the specific humidity of the first guessed profile at each level for the subsequent iteration ($q_{v_{i+1}}^{mod}$). The iterative process is repeated until the constructed profile deviates 0.1% from (IWV^{obs}) or after 20 iterations.

$$q_{v_{i+1}}^{mod} = q_{v_i}^{mod} \cdot \frac{IWV^{obs}}{IWV_i^{mod}} \tag{1}$$

The simulated model state at the time step when new observations are issued, is then nudged towards the constructed specific humidity profiles, as described in Eq. 2. The assimilated state of the variable at a specific time and location, $q_v(\vec{x},t)$ departs from the state of the model numerics and physics, $F(\vec{q_v}, \vec{x},t)$, and depends on the difference between the simulated variable and the observations $\left(q_{vk}^{obs} - q_v(\vec{x_k},t)\right)$ The nudging equation also depends on the nudging coefficient, G_{q_v} that imposes a relaxation in time of $6 \cdot 10^{-4} s^{-1}$ corresponding to an e-folding decay of 30 min for the observations. $W_k(\vec{x},t)$ is the observation-dependent weight, that spreads the information spatially and assigns a weight to each observation type depending on their quality and representativeness. In other words, grid points further from the station location and observations with lower quality are weighted less in the nudging process. The suffix k corresponds to each observation type (in our case it is just the GPS observations). Further details of the nudging procedure can be found in the model documentation (Schraff and Hess, 2012) and in Caldas-Álvarez and Khodayar (2020) and Caldas-Álvarez et al. (2021).

$$\frac{\partial}{\partial t} q_v(\vec{x},t) = F(\vec{q_v}, \vec{x},t) + G_{q_v} \cdot \sum_{k(obs)} W_k(\vec{x},t) \left[q_{vk}^{obs} - q_v(\vec{x_k},t) \right] \tag{2}$$

3. Methodology

We run two sets of simulations, first, we run seasonal hindcasts with COSMO-CLM and no data assimilation at horizontal resolutions of 7 km and 2.8 km of the HyMeX Special Observation Period 1 (SOP1), i.e., from 01-Sep-2012 to 20-Nov-2012. The simulations of this set are hereafter named CTRL-7 and CTRL-2.8, depending on the model resolution. The second set consists of COSMO-CLM hindcasts of the same period, model physics, and forcing data where the only difference is the assimilation of GPS-ZTD data using the Nudging Scheme. We refer to these simulations as NDG-7 or NDG-2.8, depending on the model resolution. The rationale behind these experiments is to allow a selective comparison of the

impacts of GPS-ZTD nudging on heavy precipitation, avoiding spurious interferences from other sources, e.g., different forcing data or model settings. To ensure the comparability of both sets of simulations we employ the same forcing data. Both CTRL-7 and NDG-7 are forced by analyses of the Integrated Forecast System (IFS) of the European Centre for Medium-Range for Weather Forecasts (ECMWF) at a 0.25° resolution. For its part, CTRL-2.8 and NDG-2.8 are forced by the CTRL-7 simulations in a one-way nesting strategy. Fig. 1 shows the simulation domains of CTRL-7 and NDG-7 (blue) and CTRL-2.8 and NDG-2.8 (green). We select these simulation domains as they show the largest coverage of the employed observational data sets (Fig. 1). A single simulation is run for CTRL-7 and NDG-7, respectively, encompassing all western European countries, a vast region of the Atlantic Ocean, and northern Africa. On the contrary, we perform three different simulations at 2.8 km over the Iberian Peninsula (IP), France (FR), and Italy (IT) to reduce computational costs. Hence the CTRL-2.8 and NDG-2.8 simulations over IP, FR, and IT are independent of one another.

We define 3 regional investigation domains for process-based analysis, IP, FR, and IT. These three investigation domains are centred over the previously defined IP, FR, and IT simulation areas skipping 4 grid points at each of the boundaries to avoid including artefacts created by the proximity of the sponge layers. Regarding local investigation domains, we work with the 8 HyMeX-defined target areas Valencia (VA), Catalonia (CA), Balearic Islands (BA), Cevennes-Vivarais (CV), Corsica (CO), Northeastern Italy (NEI), Central Italy (CI) and Liguria-Tuscany (LT), for reference see Ducrocq et al. (2014).

4. The impact of GPS nudging on the atmospheric moisture field

4.1. Model representation of atmospheric moisture across resolution in comparison with observations

To assess the modelling accuracy of the spatiotemporal distribution of atmospheric humidity the seasonal simulations with the COSMO-CLM model covering the autumn period of 2012 are compared against GPS and radiosounding information. Previous comparisons between both systems showed GPS performance against radiosondes to be in line with previous bias estimations, differences not higher than 2 mm are identified (not shown).

In a local-to-regional approach, the three climatic subdomains (FR, IP, IT) and 8 target areas (TGA) described in section 3 are considered (Fig. 1). Our purpose in this section is to answer the following questions, (a) How accurate is the model representation of the atmospheric humidity? Are there any biases in relation to specific periods/regions? (b) How affects the modelling grid resolution, the water vapour representation and related processes?

Fig. 2 shows a temporal evolution of spatially averaged daily IWV ranging between 32 mm and 7 mm, generally for the three areas. No relevant differences are observed in this analysis between CTRL-7 and CTRL-2.8. The comparison of the temporal and spatial distribution of the seasonal mean between GPS-derived IWV and COSMO-CLM values over the WMed subdomains and TGA reveals a wet bias across resolution (Figs. 2b and 3). Fig. 2 shows that biases in daily IWV can be as large as −7 mm with a general wet bias of ca. 2 mm (lower panels of Figs. 2a to 2c). This is a well-known issue by the COSMO model pointed out in past literature for coarser-resolution simulations (Schraff et al., 2008; Cress et al., 2012; Devidasrao, 2012), which persists in the finer grid runs (Caldas-Álvarez and Khodayar, 2020; Caldas-Álvarez et al., 2021).

The three selected subdomains show a temporal mean bias of about −0.4 to −1.3 mm and in the order of 0.2 to −1.9 mm for the TGA and a spatial mean bias between 1 and 1.6 mm for IP, FR and IT, with maximum differences up to 10 mm on daily and sub-daily time scales (Fig. 2). The convection parameterized and the explicitly resolved simulations show similar performance. Locally, CO and CI show the worse metrics in the reference simulations probably because of their exposure to maritime flows, their complex topography and the GPS coverage gaps

e.g., in Tuscany and Campania regions in CI. Similar performance is observed across resolution. In the period under investigation, a contributor to the wet bias in the simulation domain is found to be the occurrence of four sub periods of excessive advection and evapotranspiration over Spain, northern Africa, Corsica, and Sardinia contributing to the excessive moistening of the atmosphere in COSMO-CLM as identified by comparisons against GLEAM and MODIS products (for details see Caldas-Álvarez and Khodayar, 2020).

In addition to the generalized wet bias, the spatial distribution of daily IWV differences averaged over the period of investigation reveals a persistent dry bias over mountainous regions, such as the Pyrenees, the Alps, and Corsica (Fig. 3). The nudging of the GPS-ZTD has a direct positive impact on the overall seasonal wet bias. The temporal and spatial mean absolute bias is reduced (from about 1.3 mm to 0.8 mm), and the general metrics improve, RMSE (from about 1.8 mm to 0.5 mm) and the AI (from 0.97 to 0.99). However, little impact is seen over the dry bias of the complex areas where large differences persist at both resolutions after nudging. These differences could be in relation to the small discrepancies between the surface height in COSMO-CLM and the GPS measurements despite the quality control and flags applied to the observational data set before applying the nudging methodology. The positive deviations can be as large as 5 mm in the COSMO_CLM-7 km and lower, about 3 mm in the COSMO_CLM-2.8 km. The latter agrees with the more realistic representation of topography in the finer resolution model, thus pointing out the benefit of higher resolution modelling for an improved model representation of atmospheric moisture over complex terrains.

4.2. Impact of corrections on atmospheric moisture

The subdomains more largely affected by the nudging, with a general IWV reduction in the order of 10%, are FR and IP, showing IT the weakest response, about 3–8% decrease in total column atmospheric moisture (not shown). This can be explained by the large number and density of stations deployed over the IP domain (359) and particularly FR (259), contrary to the low number of GPS stations over IT (191) in addition to the large underestimation over elevated stations of the Alps. Moreover, the Italian Peninsula is located downstream of Africa and the Mediterranean Sea, regions of very low or no GPS coverage. Thus, dominant flows in this domain from the southwest, south, and eastern areas transport no bias-corrected air masses. This highlights the remote impact of GPS nudging, in addition to the local implications, through the advection of air masses by the dominant flows in the region. Furthermore, over the Mediterranean Sea, despite the lack of GPS-nudging an effect is observed offshore where a general reduction of about 2% is also registered (difference between the NDG and CTRL simulations). This is a consequence of the spreading of the nudged information in the horizontal dimension as well as the redistribution of atmospheric humidity by advective processes in the region. At a local scale, the weakest impact is also over CO and CI (Fig. 1), areas particularly exposed to maritime flows. Nonetheless, maximum differences after nudging are below 2 mm in all subdomains and at both resolutions, being the positive impact larger on the finer resolution simulation.

The simulated probability of extreme IWV values and the diurnal cycle was additionally affected by the atmospheric moisture correction and the subsequent general drying of the atmosphere. The probability distribution Function (PDF, Fig. 4a) of the timely averaged IWV spatial distribution (Fig. 3) shows in all subdomains a shifting of about 2 mm in the mean towards lower values, in line with the wet bias correction shown in Figs. 2 and 3. In all subdomains, a slight probability increase is observed up to 10 mm and markedly decreases above 20 mm, indicating a reduction of total moisture content and a shift of the distribution towards more moderate values in the NDG. The probability of the most extreme values decreases (Fig. 4a), where larger deviations between REF and NDG simulations at both resolutions occur from about 25 mm, with reduced and analogous probability for the NDG simulations. The daily
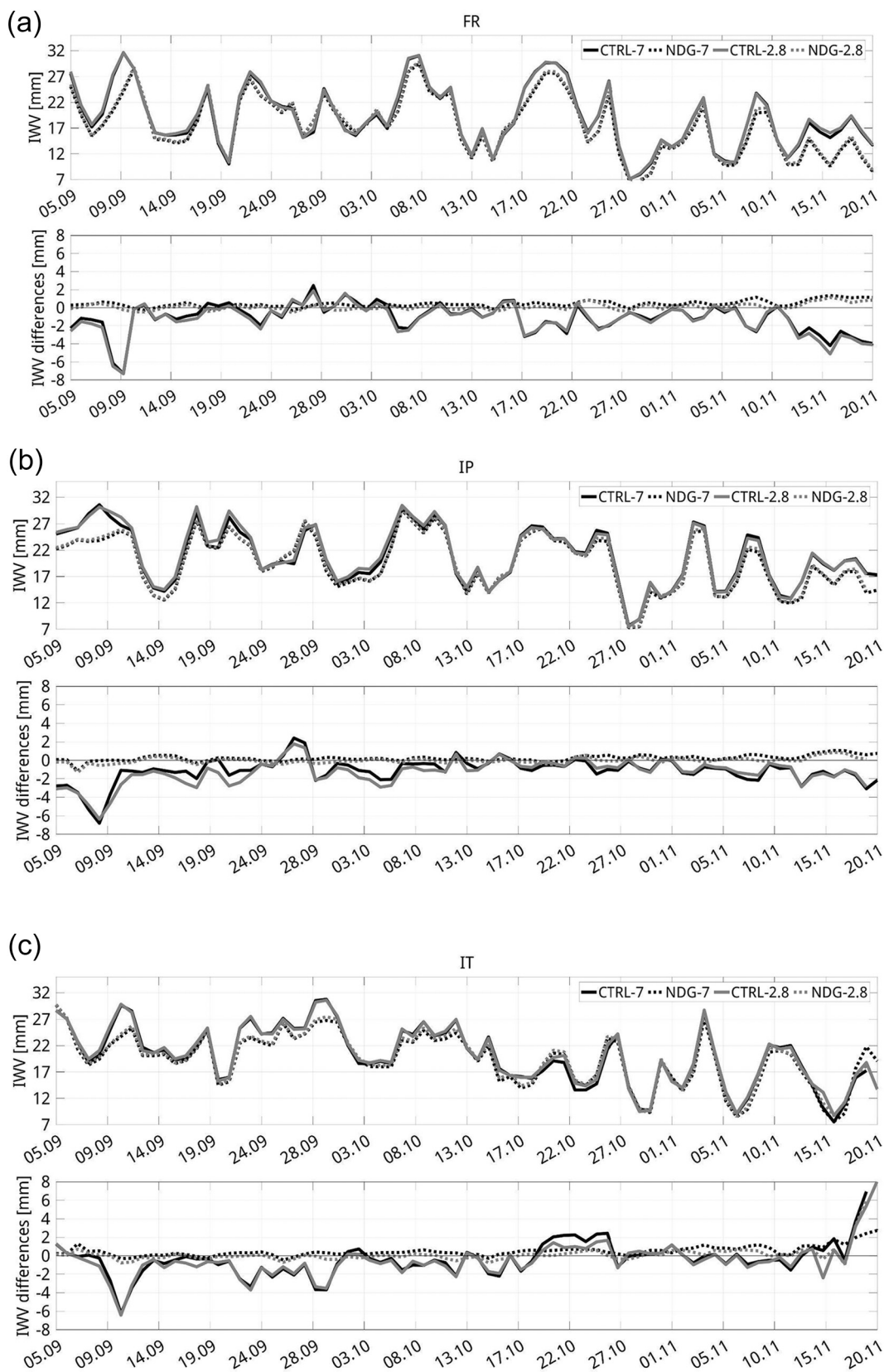
Fig. 2. Temporal evolution of the area-averaged daily mean of IWV (upper row) and differences at the location of the GPS station measurements (lower row) for FR (a), IP (b), and IT (c). The differences against the GPS measurements are obtained as OBS-MOD, hence negative values correspond to the simulations being wetter than the observations. IWV at the GPS location is obtained through bilinear interpolation.

(a)
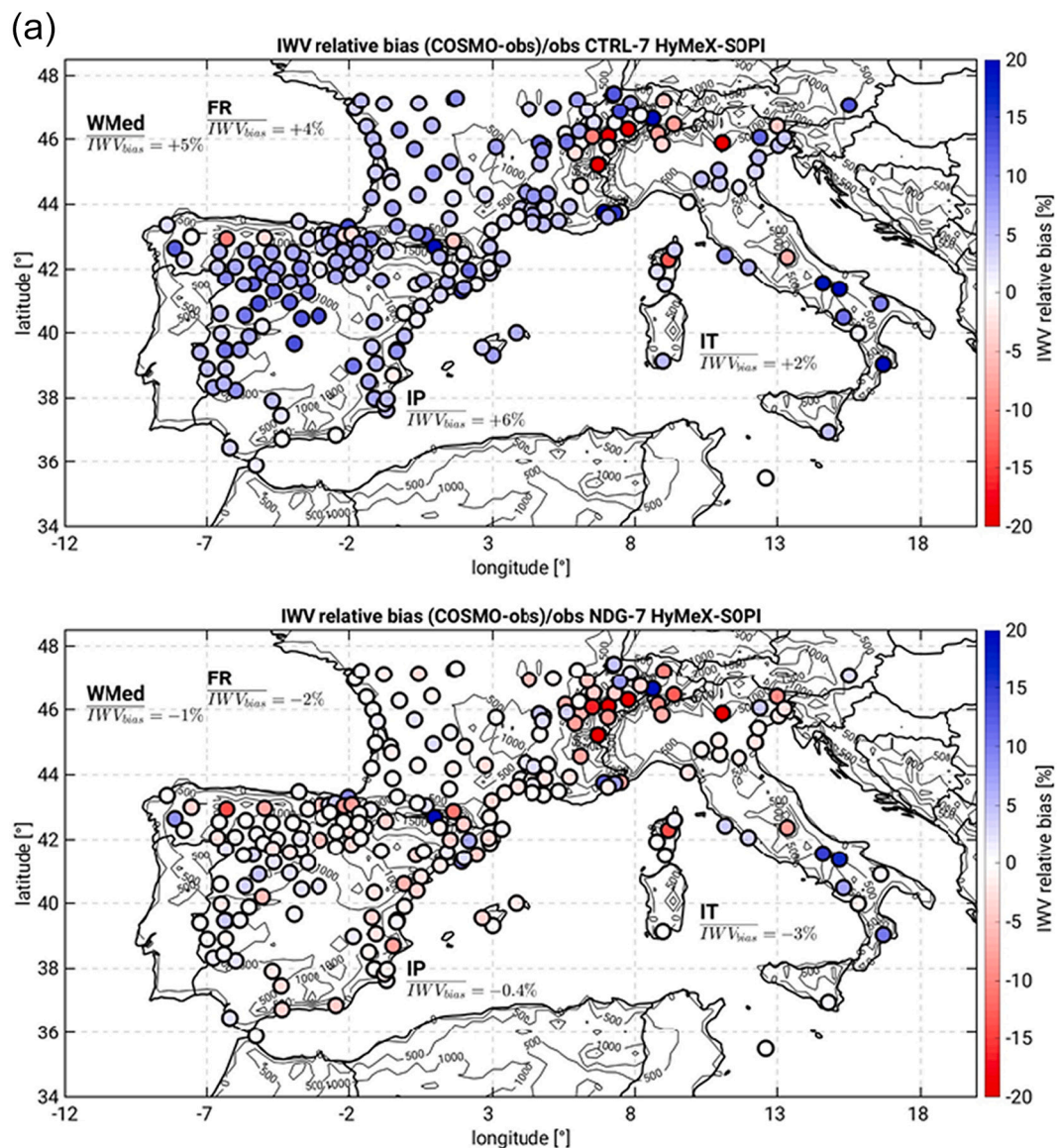
Fig. 3. Percentage bias of simulated daily mean IWV against GPS-IWV for the period of study and at the location of the GPS stations. (a) CTRL-7 and NDG-7, (b) CTRL-2.8 and NDG-2.8. The percentage mean bias for each subdomain is also indicated.

cycle of IWV illustrates the aforementioned changes (Fig. 4b), revealing a generalized decrease in atmospheric moisture and an intensification of the cycle contributing to the correction of the mean diurnal cycle. Interestingly, the nudging reduces the amount of IWV by 1.5 mm in the early morning and by only 0.5 mm in the midday and afternoon for both resolutions and all subdomains pointing out not only a general wet bias in the model simulations but also deficiencies in the diurnal cycle relevant for the building of the precipitation diurnal cycle in the model.

Despite the integrated nature of the GPS-derived information, the impact of the consequent atmospheric moisture reduction is reflected in the model simulations throughout the complete atmospheric profile. The redistribution of information in the vertical direction is in this case performed based on the existing model profiles. To assess the impact of the nudging, comparisons with soundings from operative stations, providing information every 6 h to 12 h, are performed. In Fig. 5, examples for 3 stations, namely, Barcelona (Spain, IP), Nimes (France, FR), and Pratica di Mare (Italy, IT), are shown. These comparisons should not be considered representative of the whole climate domain; however, they are expected to provide an estimation of the impact of the nudging

on the vertical stratification of atmospheric humidity. Between 50 and 80 soundings, depending on the availability at each station, are used for this validation exercise. The mean squared difference at 11 pressure levels is shown, where the sounding data has been interpolated vertically to those 11 levels and the COSMO-CLM specific humidity values are taken from the closest grid point to the station location. The comparison over the 3 stations shows a reduction of the RMSE between 500 hPa and the 950 hPa at both resolutions, meaning an improvement in the vertical stratification of atmospheric moisture in this layer. However, below 950 hPa in Pratica di Mare and Barcelona, an improvement is seen, whereas a worsening is observed in Nimes. This is probably a consequence of the expected humidity reduction in the whole profile due to the nudging of column moisture, which corrects the original model overestimation present above the 950 hPa but exerts a worsening effect over the already too dry lower troposphere below this level. Dry biases in the order of 1.5 to 2.5 g/kg are identified in Nimes at 1000 hPa for the NDG-7 and NDG-2.8 simulations, larger by about 0.5 g/kg than their counterparts. Furthermore, the observed impact in the lower-atmospheric levels is due to the nudging procedure itself, given, for
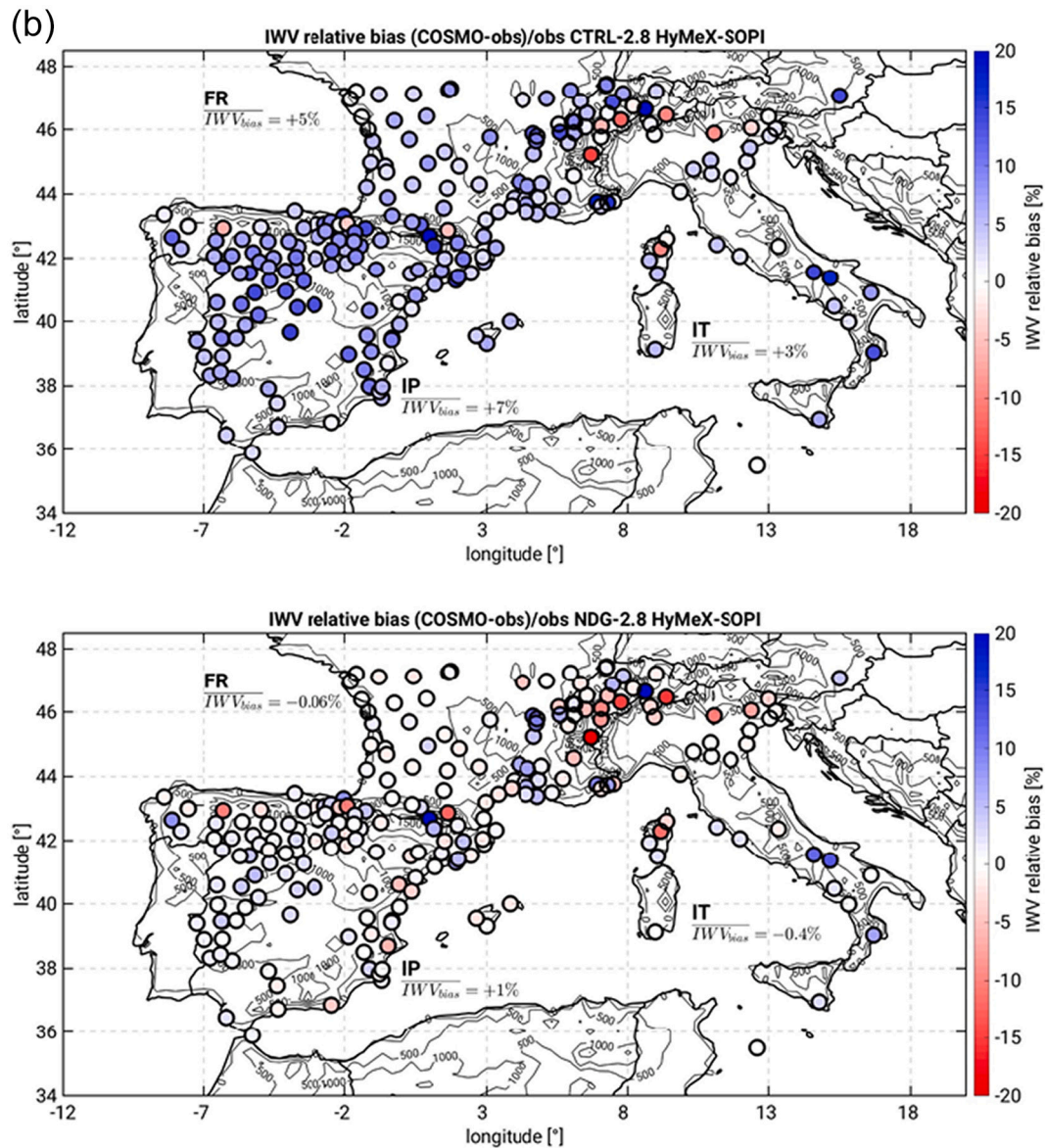
Fig. 3. (*continued*).

humidity corrections inducing relative humidity over 100%, it truncates the specific humidity amount to the saturation point. Since most of the selected stations are at low altitudes near the coast, and are frequently affected by maritime flows, the corrections induced by the GPS-ZTD nudging at the PBL occur often in an already saturated environment. This is especially the case during midday and the afternoon.

5. Sensitivity of atmospheric conditions to the moisture corrections

In Caldas-Álvarez (2019) it was shown in a detailed examination of the relationship between total column atmospheric moisture and heavy precipitation in all intensive observation periods (IOPs) during the SOP1 of HyMeX, regardless moisture corrections, that in 90% of the SOP1 events an IWV increase precedes heavy precipitation occurrence (between 1 h and 12 h prior to precipitation start), being the most intense events related with the largest increases (> 10 mm) and the longer build-up times (about 30 h). Regarding the impact of the atmospheric moisture correction, about 70% of the cases, at both resolutions, a positive IWV-precipitation causality exists. This means that the most probable cause is

that of an increase(reduction) in mean IWV before the precipitation starts, followed by an increase(reduction) in the precipitation amount.

These results highlight the intrinsic relationship between atmospheric moisture and precipitation in the region, thus the expected high sensitivity of atmospheric conditions leading to heavy precipitation to moisture variations. This section aims at examining the impact of the moisture corrections on the atmospheric chain of convection-related processes leading to heavy precipitation considering the local-to-regional characteristics of the studied domains and the implications of using convection parameterized versus explicitly resolved simulations. In Fig. 6, the spatial distribution of seasonal averaged relative differences (NDG-CTRL) of relevant variables are seen, while in Fig. 7 by means of box-and-whisker plots part of this information is summarised.

5.1. Temperature, humidity at the near-surface and surface turbulent fluxes

The generalized decrease in atmospheric moisture content impacted the whole region in all domains under study (Figs. 6a and 7 (IWV)). This affects the exchange of heat and moisture at the ground-atmosphere
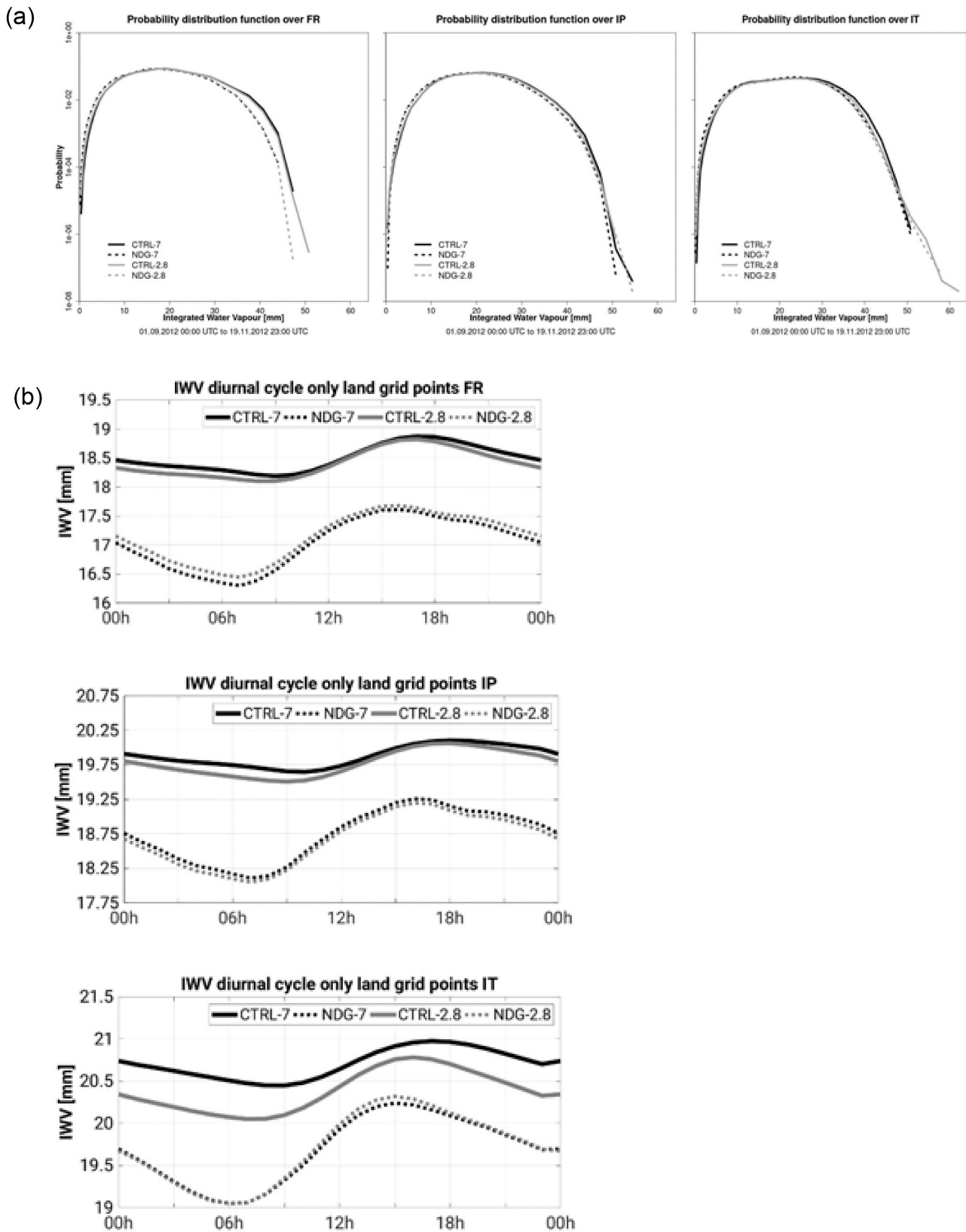
(a)

(b)

Fig. 4. (a) Probability distribution Function (PDF), and (b) daily cycle of hourly simulated IWV, for the whole period of study, over the IP, FR, and IT (please be aware of the different x-axis IWV scale). Only land points are considered.
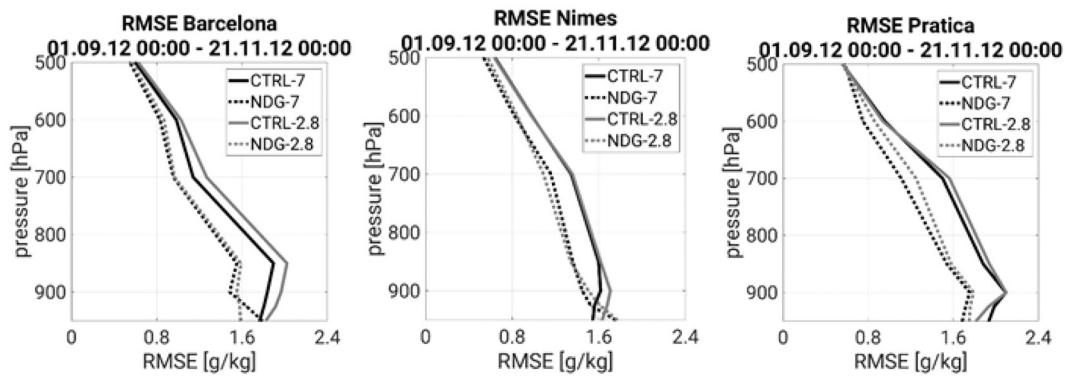
Fig. 5. Vertical distribution of specific humidity RMSE between operational soundings and simulated COSMO-CLM profiles, at three locations within the climatological subdomains under investigation, Barcelona in IP, Nimes in FR and Pratica in IT.
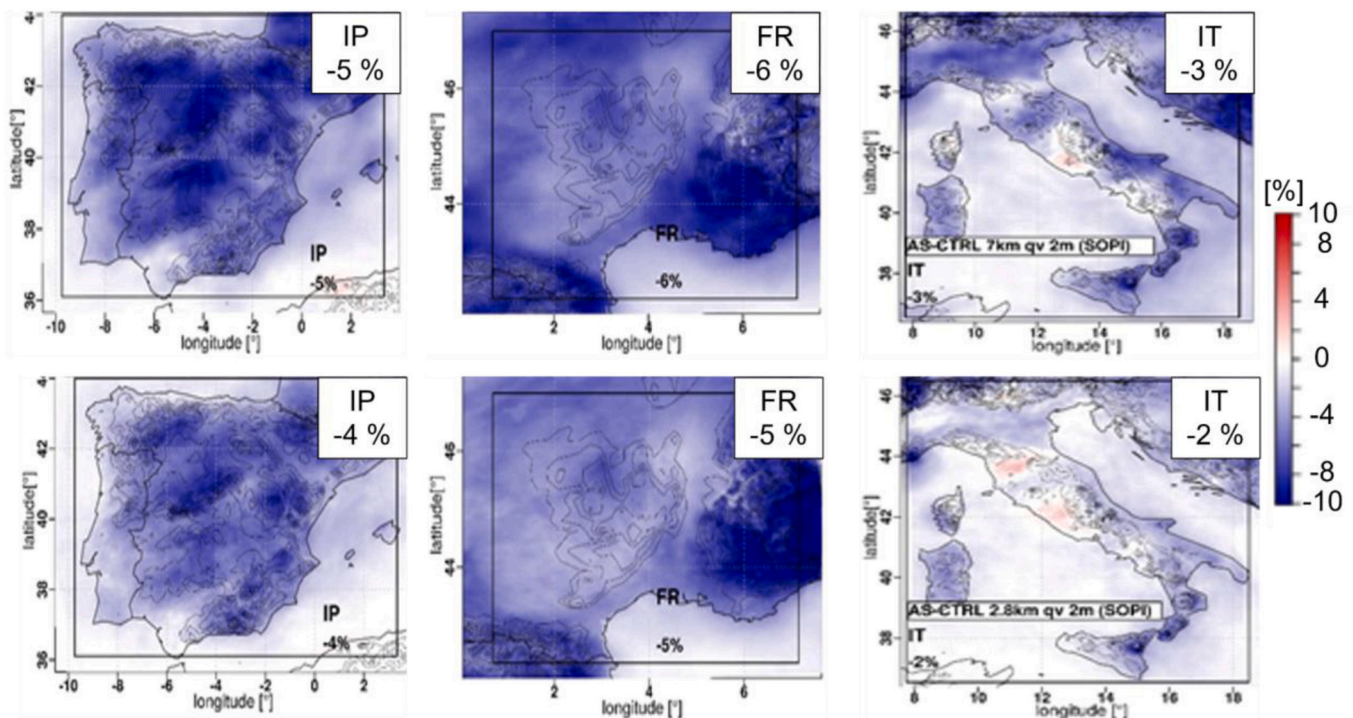
Fig. 6. Spatial distribution of seasonal averaged relative differences (NDG-CTRL) of the following, (a) 2 m specific humidity, (b) latent heat flux, (c) 2 m temperature, (d) CAPE, (e) total cloud cover, (f) geopotential height, and (g) precipitation. The panels in the upper row show 7 km differences and panels in the lower row indicate differences in the 2.8 km simulations.

boundary through the changes of humidity, but also indirectly by the redistribution of atmospheric moisture and changes in precipitation and radiation (through modified cloud cover) on larger spatiotemporal scales given the seasonal nature of the investigated period. The inhomogeneous response, also influenced by the types of surfaces, in the surface turbulent flux fields (Fig. 6b) across resolution contrasts with the homogeneous decrease in 2 m specific humidity (mean 0.5 g/kg, mainly over IP and FR due to the larger GPS coverage). However, a large agreement exists between the 2 m temperature seasonal mean variations and the sensible heat flux changes in overall climatic subdomains and grid resolutions. COSMO-CLM acted to balance the total net radiation at the surface in turn affecting 2 m temperature (Fig. 6c). Given the drying effect of the nudging of column moisture affected mainly the low-level homogeneous terrains, complex areas and water bodies emit more

latent heat flux. Particularly in these areas changes in the surface fluxes were controlled by changes in the seasonal precipitation patterns. The response is similar at 7 and 2.8 km, but the contrast is weaker at 2.8 km. There are also regions, such as the Thyrrenean Sea or the Guadalquivir valley, less affected by the nudging in relation to the dominant moisture advection in the areas being from the southwest, locations with no GPS coverage. The Sea is also largely affected despite the lack of GPS stations due to the horizontal spread of the nudging effect and the transport by the wind flow.

5.2. Atmospheric instability and cloud cover

A direct impact on the atmospheric instability is shown by the reduction of CAPE and absolute KO-index (Figs. 6d and 7). This effect is
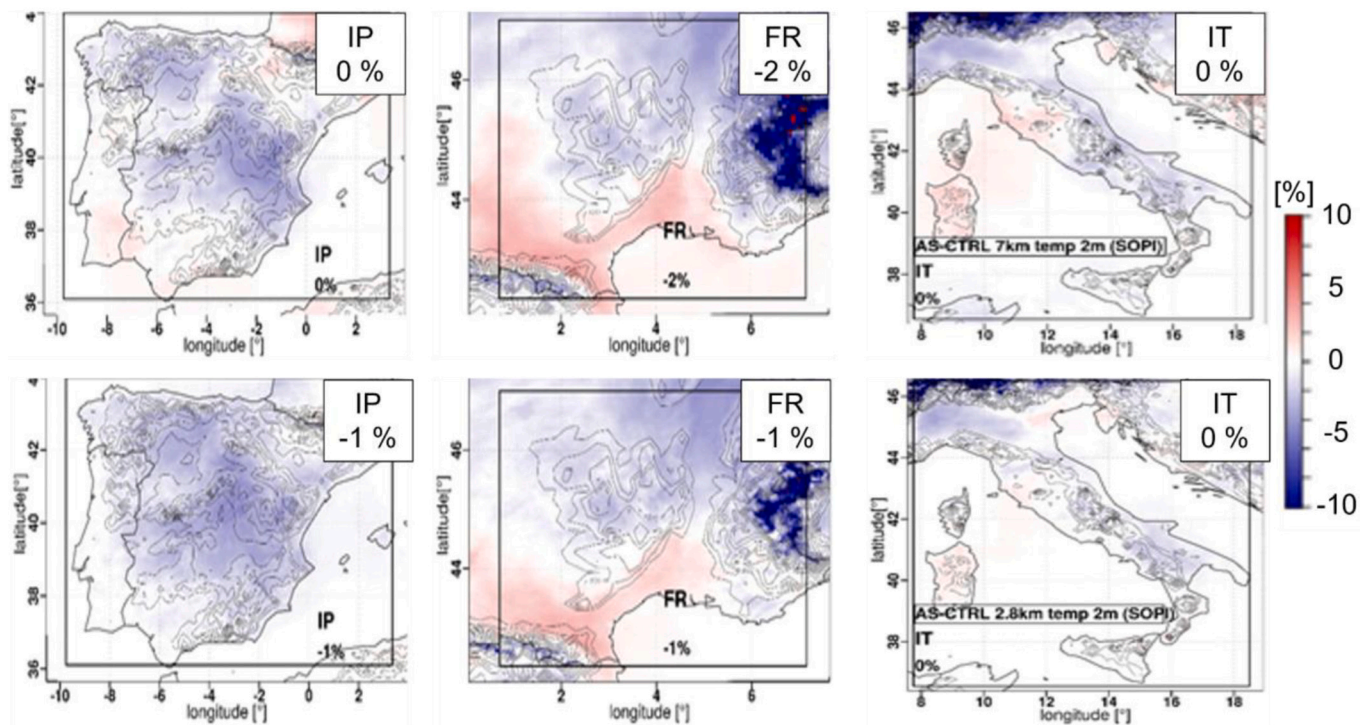
b) Latent Heat Flux
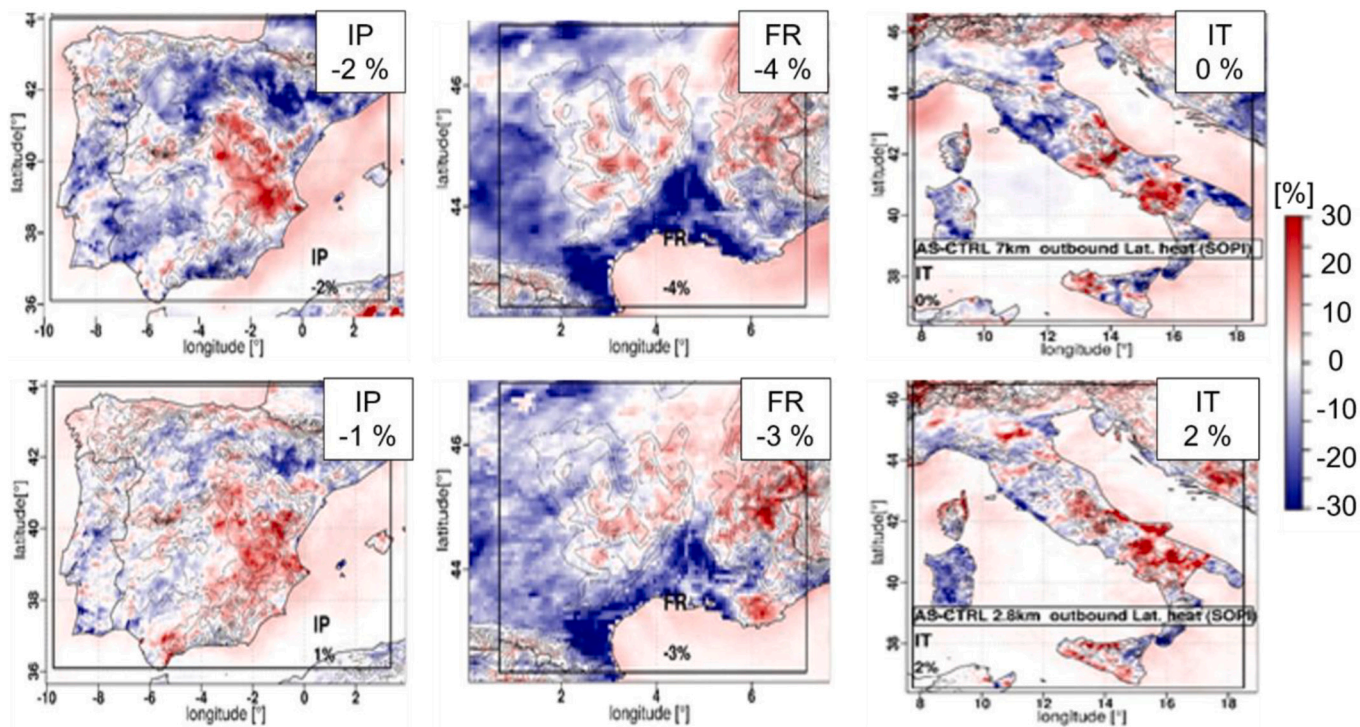
c) 2m temp

Fig. 6. (*continued*).

seen in the seasonal means, but also for sub-seasonal selected episodes (Caldas-Álvarez and Khodayar, 2020). Large mean CAPE reductions occur over the Sea, about 75 J/kg, and overland, about 50 J/kg. This impact is a direct consequence of the atmospheric humidity reduction by the moisture nudging particularly in the lower-atmospheric levels, specific humidity at 2 m since the calculation of the CAPE mean layer method is particularly sensitive to variations in atmospheric conditions in the lower troposphere. This impact entails consequences for the

d) CAPE
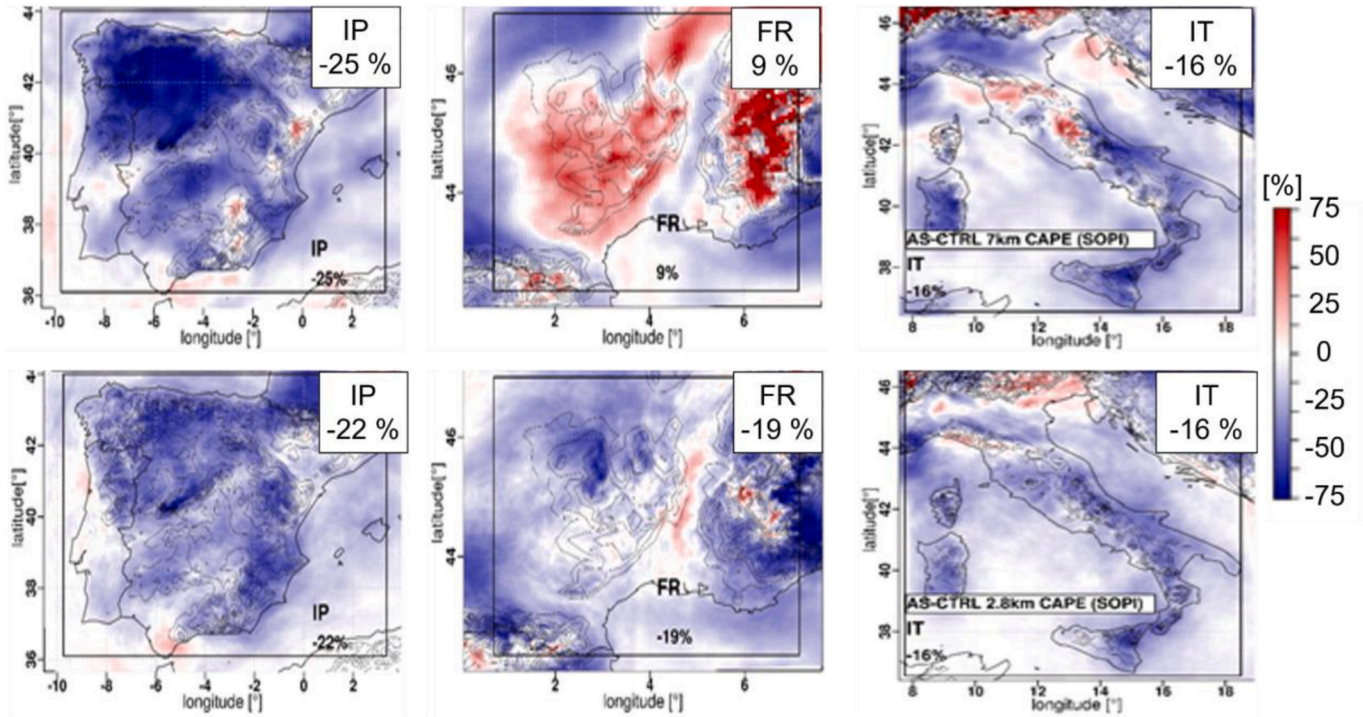
e) Total cloud cover
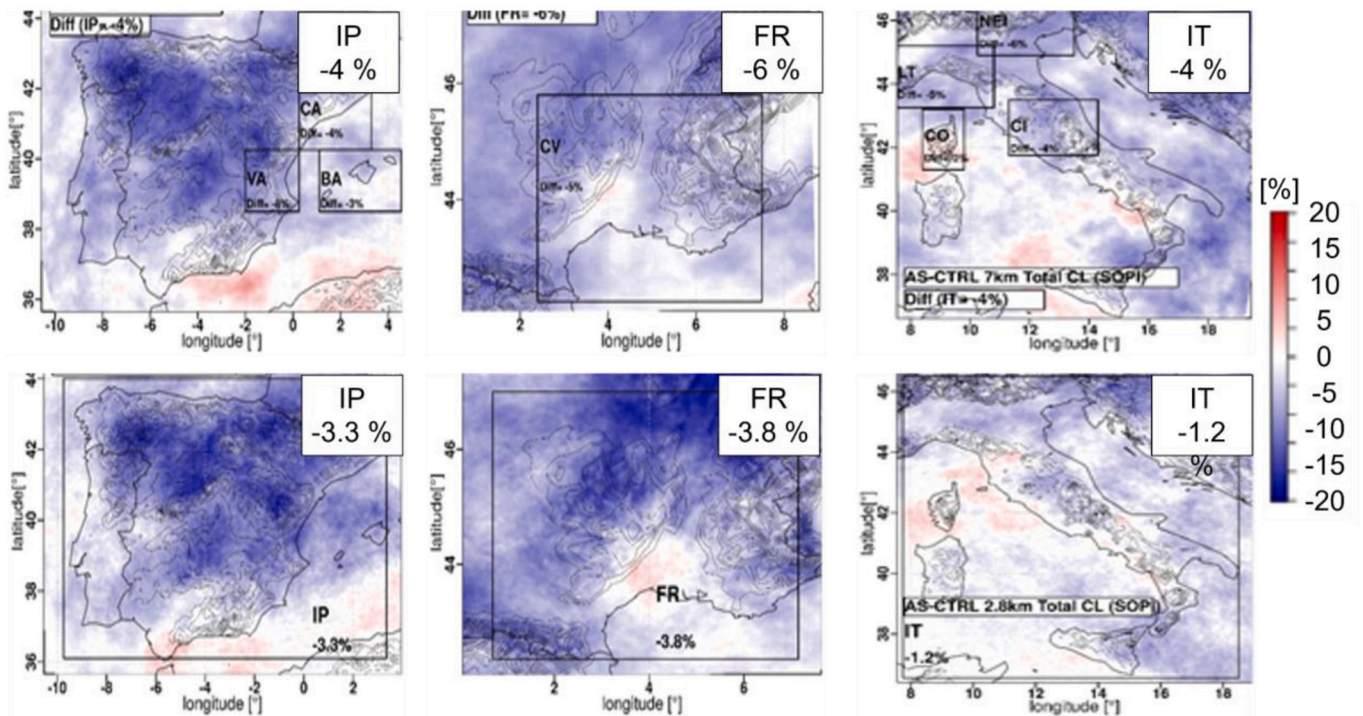
Fig. 6. (*continued*).

buoyancy of lifted parcels, the height of significant convection-related levels such as the lifted condensation level (LCL), level of free convection (LFC), and equilibrium level (EL), which define the development of convective clouds (not shown). The reduced instability and the reduced tropospheric moisture hindering deep moist convection contribute to the reduction of cloud cover at low- and mid-levels. The strong reduction of the cloud cover in all subdomains is about 4% and takes place at both resolutions (Fig. 6e).

f) 500 hPa geopotential height
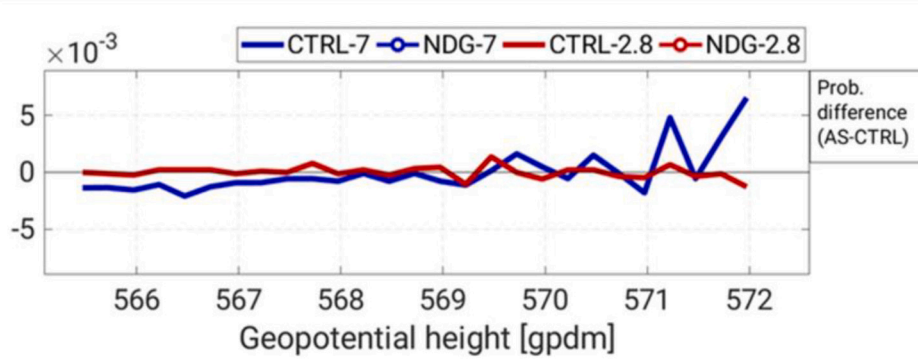
g) Precipitation
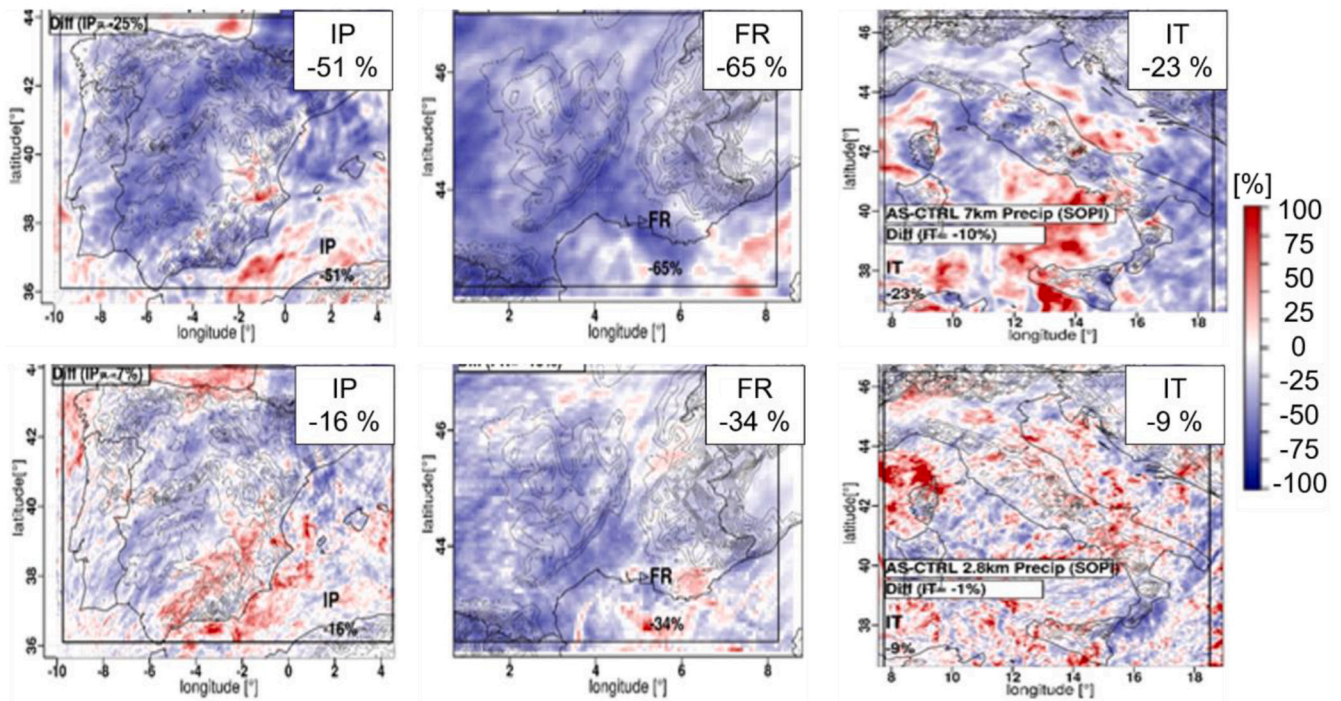
Fig. 6. (*continued*).

5.3. Large-scale pressure

The column atmospheric nudging impacted the large-scale distribution of low-pressure systems. Regarding the 500 hPa geopotential height (Fig. 6f), larger values are more probable in the NDG simulation. Under cooling or drying of the atmospheric column, surface pressure builds up, lifting accordingly the geopotential height at 500 hPa. Although mean differences are low, it has been demonstrated in Caldas-Álvarez and Khodayar (2020) that even these small changes have a significant impact on wind circulations, hence, on convergence/divergence fields and triggering of convection, thus, on the moisture transport.

5.4. Precipitation

The nudging of atmospheric moisture information yielding a drying of the atmosphere to balance the general wet bias of the model, leads to a general reduction of seasonal mean precipitation at both resolutions (Fig. 6g and 7). Contrary to the generalized reduction inland, some

regions show an increase in the mean precipitation such as some areas of the Med Sea. The spatially averaged relative differences in seasonal precipitation amount over all climatic subdomains show a decrease ranging between −9% to −65% depending on the area and model grid. A higher reduction is seen in the 7 km because of the more accurate representation of the CTRL-2.8 km and NDG-2.8 km in comparison to observations (Figs. 2 and 3). But probably also in relation to the narrower simulation domains of the 2.8 km runs, which impede the transport of "atmospheric moisture corrected information" in remote areas towards the study areas.

The nudging of column atmospheric moisture observations brought a modification in the amount, distribution, and timing of water vapour, which in turn affects the atmospheric conditions, thus the precipitation field. The precipitation amount-duration plots (Fig. 8 for selected TGA) evidence that the generalized precipitation reduction affects all precipitation ranges from short-low-intensity to long-duration high-intensity precipitation.
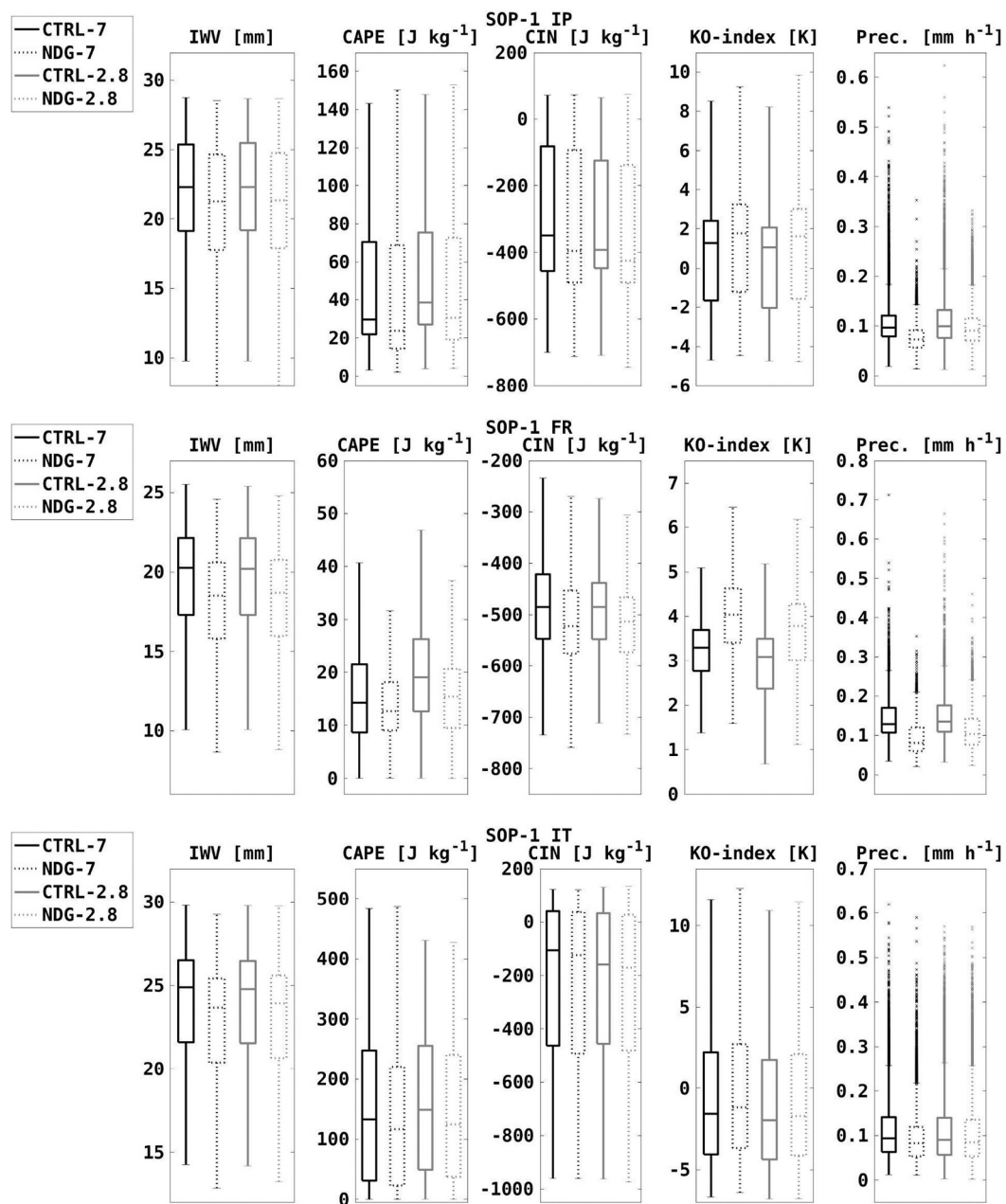
Fig. 7. Box-and-whisker plots including the median, quartiles, and extremes of IWV, CAPE, CIN, KO-index, and hourly precipitation (the dots in the precipitation panel denote the outliers, i.e., values over 90-perc). The distributions are obtained in the period 01-Sep to 20-Nov.

6. Improvement of seasonal precipitation modelling?

To evaluate the modelling performance in terms of accurate precipitation modelling the CMORPH product is used. CMORPH was chosen instead of raingauge information principally because of two aspects, a) the unavailability of information over the sea considering the latter product, and b) the already regular grid of the CMORPH product, which is convenient for the validation methodologies applied in this study. Furthermore, the evaluation of the gridded CMORPH product against rain gauges demonstrated in agreement with previous studies that this high spatiotemporal resolution product blending several microwave satellite measurements is useful for validation purposes in the western Mediterranean well capturing the areas prone to heavy precipitation in the region (e.g., Ducrocq et al., 2014; Lionello, 2012). In this case, only above the Alps, CMORPH shows a too weak probability of precipitation above the percentile-90, about 10%, which is too low for the period

under investigation. Comparisons with the COSMO-CLM model simulations, CTRL-7 and CTRL-2.8, show an overestimation of the frequency of extreme precipitation over the IP, but an underestimation over the Mediterranean Sea and along the Balkan coast. The moisture nudging brings a better agreement with CMORPH increasing the frequency of extreme precipitation over the Mediterranean, additionally reducing the frequency over IP and FR. However, still relevant differences at both resolutions, of about 10%, remain over the Balkans (not shown).

Furthermore, using the object-based verification method, Structure-Amount-Location (SAL, Wernli et al., 2008), which quantifies the accuracy of precipitation forecasts, differences regarding the three metrics Structure (S), Amount (A) and Location (L), are identified (Fig. 9) for all simulations versus CMORPH observations. In general, the moisture nudging exerts a larger impact over the IP and FR region rather than IT, probably in relation to the lower number of GPS stations in the region and the upstream MedSea inflow lacking the large impact of local
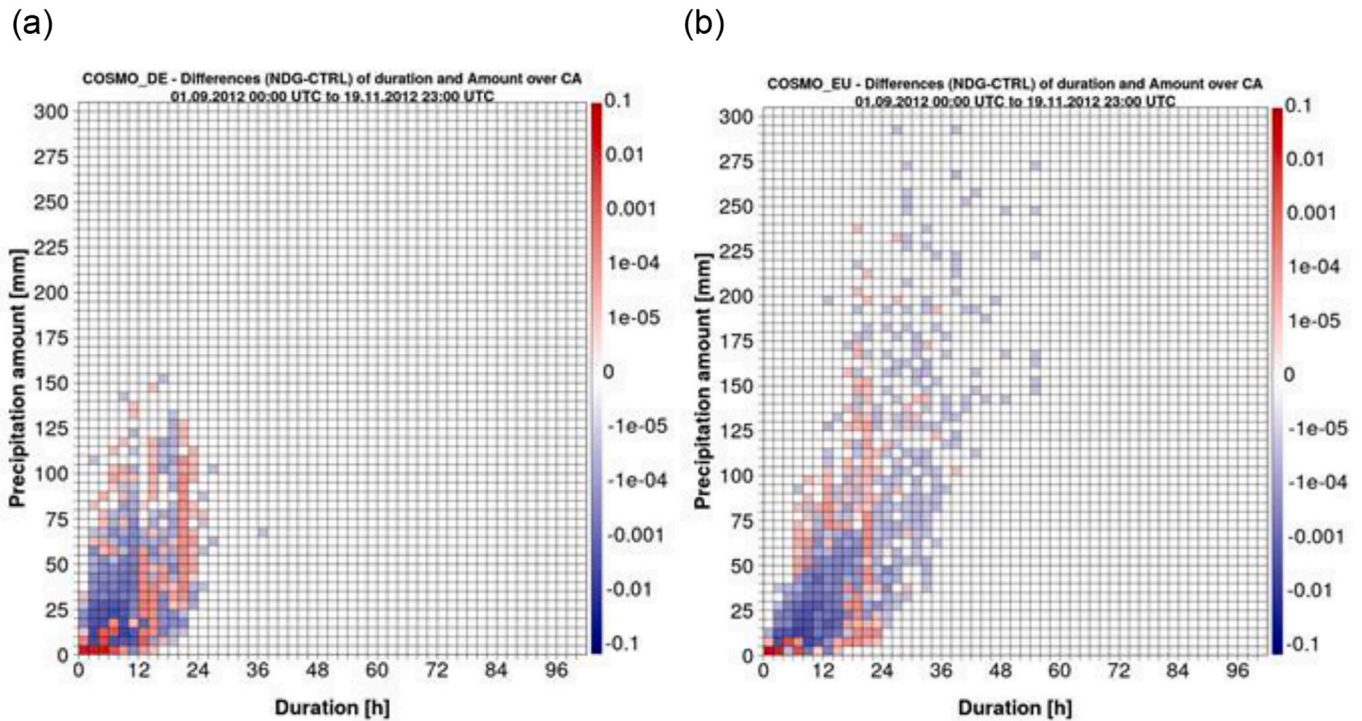
(a)

(b)

Fig. 8. Illustrative difference plot (NDG-CTRL) of duration versus amount of hourly precipitation for the selected TGA CA in SP. (a) COSMO-DE, and (b) COSMO-EU, 1.09.2012 to 19.11.2012.
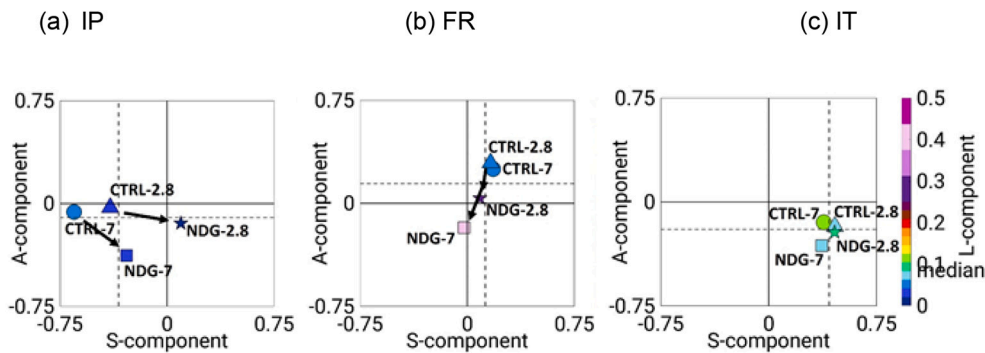
(a) IP   (b) FR   (c) IT

Fig. 9. SAL (Structure-Amount-Location) verification method applied to the timely mean of the COSMO-CLM precipitation and CMORPH observations over the whole study period. The closer the metrics to zero, the better the agreement between the precipitation field from CMORPH and COSMO simulations.

nudging information. The mean reduction of the precipitation amount at both resolutions in all climatic domains turns out to be beneficial for FR, but detrimental for IP and IT. Regarding the precipitation structures, an improvement is observed for both resolutions overall climatic domains, IP, FR, IT. Albeit the improvement is rather weak over IT. The location component is improved for IP and IT but deteriorated for FR particularly at 7 km. The combined use of the explicitly resolved grid length and the moisture nudging brings the best agreement with the observations as compared to the CMORPH gridded product.

The Probability Distribution Function (PDF) of hourly precipitation shows in agreement with previous studies (Kendon et al., 2017; Fosser et al., 2015) an increased and more accurate probability for heavy precipitation when using the explicitly resolved 2.8 km runs. This is true for all climatic subdomains (Fig. 10). This difference remains after the assimilation. The runs with a 2.8 km horizontal resolution showed the best agreement with the CMORPH data set. This also remains after assimilation. After the nudging, following the generalized atmospheric moisture reduction previously described the impact at both resolutions and all regions is a reduction of the precipitation intensities at all ranges

in agreement with duration-amount precipitation diagrams in all TGA (Fig. 8) and. This precipitation reduction results, especially at 7 km and for the FR domain, in a worsening of the simulation of the precipitation events for the experiments with data assimilation. This is particularly evident for FR, probably again in relation to the high number of stations in the area in comparison to IP and IT.

The diurnal cycle of precipitation (Fig. 11, exemplary the IP is shown) reveals larger hourly mean precipitation values for the 2.8 km runs in agreement with the PDF, as compared to the convection parameterized simulations CTRL-7. The moisture nudging induces a reduction in precipitation with a strong impact/good correction of the early morning precipitation and a weaker reduction/enhancement of the late afternoon precipitation maximum. This increases the agreement of the diurnal cycle magnitude and phase with observations. The clear improvement of the NDG-2.8 km run occurs in all subdomains investigated, pointing out the potential for improvement of the precipitation diurnal cycle by combined use of high-resolution atmospheric humidity observations and fine convection-permitting simulations, this last point in agreement with previous studies highlighting the positive impact on
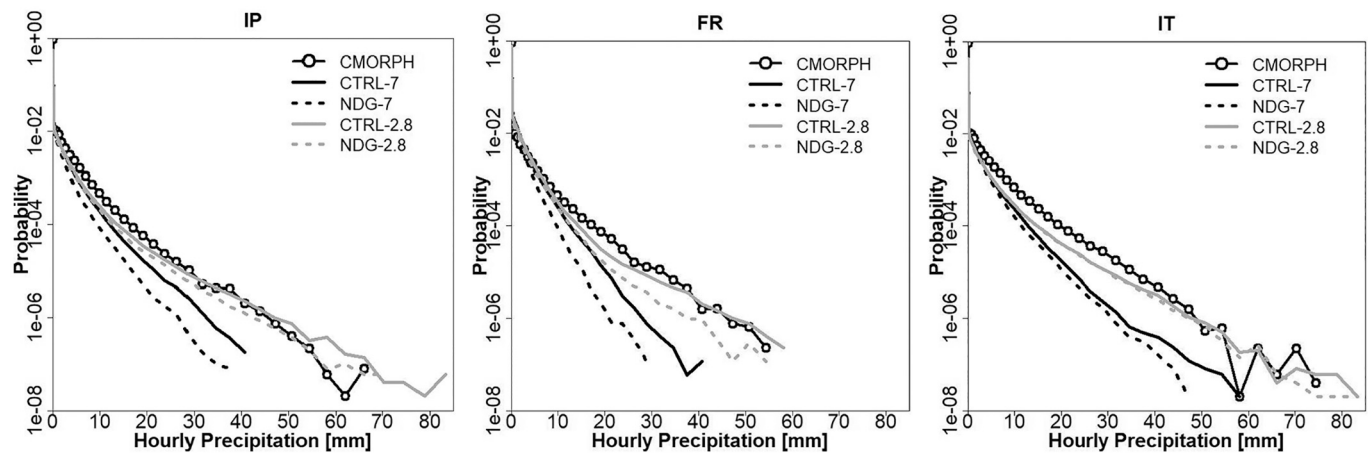
Fig. 10. Probability distribution function (PDF) of hourly simulated precipitation including CMORPH satellite observations, for the whole period of study, over the IP, FR, and IT. Only land points are considered.
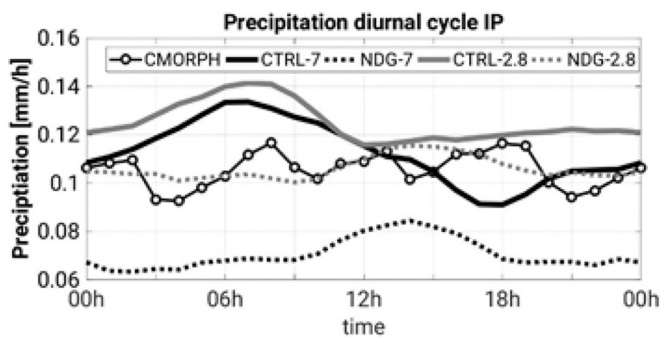

Fig. 11. Daily cycle of hourly simulated precipitation including CMORPH satellite observations, for the whole period of study, over the IP. Only land points are considered.

the diurnal cycle modelling of precipitation by reducing the horizontal grid length (Fosser et al., 2015; Birch et al., 2014; Zhang et al., 2016).

7. Discussion and conclusions

An accurate model representation of atmospheric moisture distribution, stratification, and evolution has been pointed out as key to adequately model moist convection and consequent heavy precipitation, thus, supporting prevention and adaptation measures to ameliorate fatal consequences of related high-impact weather events.

The existence of humidity biases, and their effects on model precipitation, as well as the lack of adequate observational data sets, in terms of needed spatiotemporal coverage, are common knowledge in the scientific community. Few long-term, homogeneous, sub-daily datasets of water vapour exist and none of them with full coverage of extensive regions.

In this study, we profit from a state-of-the-art Global Positioning System-Zenith Total Delay (GPS-ZTD) data set developed during the Hydrological Cycle in the Mediterranean eXperiment (HyMeX), which covers the whole north-western Mediterranean region during the autumn period of 2012, with a 10 min temporal resolution. Through nudging experiments, we investigate the sensitivity of atmospheric conditions leading to heavy precipitation to humidity corrections on a seasonal time scale. The synergetic use of high-resolution modelling with the COnsortium for Small scale MOdelling (COSMO), in climate mode (CLM), and the high spatiotemporal resolution humidity dataset provide a unique opportunity for the examination of the atmospheric moisture-precipitation interactions on a seasonal time scale in the western Mediterranean region.

A well-known wet bias characterizes COSMO-CLM simulations, and the nudging of GPS-ZTD is of great benefit to correcting the spatio-temporal representation of IWV at 7 km (parameterized convection) and 2.8 km (convection-permitting) model resolutions, entailing a reduction of about 10% in the total column water vapour, and correcting up to 10 mm at individual stations. Especially for the 2.8 km resolution better AI and RMSE scores in the temporal resolution and an improvement of the spatial distribution over mountain regions are identified.

Regionally, the largest corrections affect FR and the IP, versus IT, pointing out the relevance of the local corrections through the number/density of GPS stations, and the remote impact correction through modifications on upstream flows typically affecting the target domains. Therefore, high-density networks over land and sea are necessary to obtain accurate corrections. Even so, the nudging is unable to remove all biases over elevated terrain (e.g., the Alps, the Pyrenees) resulting from disagreements with the ground height. In this case, the finer resolution 2.8-km simulation better resolves this situation given its improved representation of the topography.

A more realistic moisture field in the seasonal simulations reflects relevant changes in the seasonal atmospheric conditions, thus, on pre-convective environments leading to heavy precipitation, and the precipitation field itself. The model showed an interesting response to the drying of the lowest atmospheric levels (2 m-specific humidity) by enhancing the outbound latent heat flux emission over regions that persisted to be wet in the seasonal values (the sea and regions of intensified precipitation). Conversely, COSMO reduced the emission of sensible heat flux over those regions ultimately increasing the 2 m-temperature over these regions of intensified sensible heat outbound flux. The reduction in atmospheric moisture content was accompanied by an increase in atmospheric stability and total cloud cover, mostly low- and mid-level clouds. Convection is reduced and the drying of the mid-troposphere levels further lowers the intensity and amount of convection by constraining its vertical development. Large-scale conditions are also affected, impacting the distribution and characteristics of air flows over land- and sea as shown by Caldas-Álvarez and Khodayar (2020) through a modification of the wind fields, hence, the convergence/divergence field. Resulting of these changes, a large impact on the precipitation field is obtained, ultimately reducing precipitation over land (9% to 65% decreased precipitation depending on the study area and the model grid resolution). The mean reduction of mean seasonal precipitation brought closer simulated precipitation totals to observations, as well as the probability of extreme precipitation. Additionally, the correction of atmospheric moisture was found to be highly beneficial for the diurnal cycle of the finer resolution 2.8 km simulation of

precipitation. The high frequency of the nudged atmospheric moisture corrected the diurnal cycle of precipitation reducing the large maximum in the morning and enhancing the afternoon maximum with a weaker impact during this time. The precipitation amount, the structure, and the location of the seasonal mean precipitating systems improved overall climatic domains and at both resolutions rendering it highly convenient at this temporal scale. However, the Probability Distribution Function of hourly precipitation shows at both resolutions and in all regions a reduction of the precipitation intensities at all ranges following the generalized atmospheric moisture reduction.

This indicates that despite the benefit on a seasonal scale, on a sub-seasonal or event scale, the improvement in the representation of heavy precipitation turns out to be case and area dependent as already shown in previous publications by Caldas-Álvarez and Khodayar (2020) and Caldas-Álvarez et al. (2021). Furthermore, the IWV lack of vertical stratified information turns out to be a big drawback of the product limiting further corrections concerning the precipitation modelling. Despite the demonstrated benefit through the nudging of high-resolution GPS-ZTD information on the seasonal scale the model struggles to correct the vertical distribution of humidity particularly in the lower troposphere. One of the reasons behind the model inability to correct the profile of relative humidity could be related with the fact that the nudging scheme doesn't consider the background error matrix, which plays an important role in modern assimilation systems, but it is not considered in the nudging scheme. The use of a variational data assimilation scheme could avoid the further drying of already dry low-atmospheric levels.

The correction of the humidity wet bias in the seasonal simulation transfers this reduction to the whole vertical distribution. This is beneficial above 900 hPa across resolution, where a generalized over-estimation of humidity was identified, however, it further increases model deficiencies below this level where already an underestimation was observed. This is most probably one of the main reasons behind the limited improvement at sub-seasonal time scales.

Results from this study demonstrate the benefit of moisture corrections on the modelling of precipitation on a seasonal scale, pointing out (a) the need for high-density networks of GPS-derived IWV, (b) measurements over the sea, and (c) the need for accurate information regarding atmospheric humidity stratification. This later could come from radiosounding information on target areas capturing upstream flows already demonstrated to be highly beneficial at sub-seasonal scales in Caldas-Álvarez et al. (2021). Additionally, the non-systematic improvement on the sub-seasonal scale highlights the need for in-depth process understanding of the atmospheric changes underlying these situations considering the characteristics of the affected regions as well as a better understanding of tendencies in model response to systematic corrections. This will help us better understand the role of atmospheric moisture as a control on heavy precipitating convection development.

Authorship contribution statement

Both authors contributed to the analysis, discussion and refinement of this manuscript.The first author, SK conceived the study, was in charge of the overall direction and planning, and wrote the manuscript. ACA contributed with the analysis and plotting of results and performed all model simulations as part of his phD thesis supervised by SK.

Declaration of Competing Interest

The authors declare that they have no conflict of interest.

Data availability

Data will be made available on request.

References

Bastin, S., Champollion, C., Bock, O., Drobinski, P., Masson, F., 2005. On the use of GPS tomography to investigate the water vapor variability during a Mistral/sea-breeze event in southeastern France. Geophys. Res. Lett. 32, L05808. https://doi.org/10.1029/2004GL021907.

Bastin, S., Champollion, C., Bock, O., Drobinski, P., Masson, F., 2007. Diurnal cycle of water vapor as documented by a dense GPS network in a coastal area during ESCOMPTE-IOP2. J. Appl. Meteorol. Climatol. 46, 167–182. https://doi.org/10.1175/JAM2450.1.

Bastin, S., Drobinski, P., Chiriaco, M., Bock, O., Roehrig, R., Gallardo, C., Conte, D., Domínguez Alonso, M., Li, L., Lionello, P., Parracho, A.C., 2019. Impact of humidity biases on light precipitation occurrence: observations versus simulations. Atmos. Chem. Phys. 19, 1471–1490. https://doi.org/10.5194/acp-19-1471-2019.

Bevis, M., Businger, S., Herring, T.A., Rocken, C., Anthes, R.A., Ware, R.H., 1992. GPS meteorology: remote sensing of atmospheric water vapor using the global positioning system. J. Geophys. Res. 97 (D14) https://doi.org/10.1029/92jd01517.

Birch, C.E., Parker, D.J., Marsham, J.H., Copsey, D., Garcia-Carreras, L., 2014. A seamless assessment of the role of convection in the water cycle of the west. African Monsoon 119. https://doi.org/10.1002/2013JD020887.

Bock, O., Bouin, M.N., Walpersdorf, A., Lafore, J.P., Janicot, S., Guichard, F., Agusti-Panareda, A., 2007. Comparison of ground-based GPS precipitable water vapour to independent observations and NWP model reanalyses over Africa. Q. J. R. Meteorol. Soc. 133 (629 B) https://doi.org/10.1002/qj.185.

Bock, O., Bosser, P., Pacione, R., Nuret, M., Fourrié, N., Parracho, A., 2016. A high-quality reprocessed ground-based GPS dataset for atmospheric process studies, radiosonde and model evaluation, and reanalysis of HyMeX Special Observing Period, 142. https://doi.org/10.1002/qj.2701.

Boniface, K., Ducrocq, V., Jaubert, G., Yan, X., Brousseau, P., Masson, F., Champollion, C., Chéry, J., Doerflinger, E., 2009. Impact of high-resolution data assimilation of GPS zenith delay on Mediterranean heavy rainfall forecasting. Ann. Geophys. 27, 2739–2753. https://doi.org/10.5194/angeo-27-2739-2009.

Businger, S., Chiswell, S., Bevis, M., Duan, J., Anthes, R., Rocken, C., Ware, R., Exner, M., Vanhove, T., Solheim, F., 1996. The promise of GPS in atmospheric monitoring. Bull. Am. Meteorol. Soc. 77, 5–18. https://doi.org/10.1175/1520-0477(1996)077<0005:TPOGIA>2.0.CO;2.

Caldas-Álvarez, A., 2019. Atmospheric Moisture Effects on Deep Convection in the Western Mediterranean. Ph. D Thesis. https://doi.org/10.5445/KSP/1000097100.

Caldas-Álvarez, A., Khodayar, S., 2020. Assessing atmospheric moisture effects on heavy precipitation during HyMeX IOP16 using GPS nudging and dynamical downscaling. Nat. Hazards Earth Syst. Sci. 20 (10), 2753–2776. https://doi.org/10.5194/nhess-20-2753-2020.

Caldas-Álvarez, A., Khodayar, S., Knippertz, P., 2021. The impact of GPS and high-resolution radiosonde nudging on the simulation of heavy precipitation during HyMeX IOP6. Weather. Clim. Dyn. 2 (3) https://doi.org/10.5194/wcd-2-561-2021.

Champollion, C., Flamant, C., Bock, O., Masson, F., Turner, D., Weckwerth, T., 2009. Mesoscale GPS tomography applied to the 12 June 2002 convective initiation event of IHOP_2002. Q. J. Roy. Meteor. Soc. 135, 645–662. https://doi.org/10.1002/qj.386.

Cress, A., Anlauf, H., Bitzer, H.W., Rhodin, A., Schraff, C., Helmert, K., Stephan, K., 2012. Global and regional impact studies at the German weather service (dwd). In: 5th WMO Workshop on the Impact of Various observing systems on NWP, Sedona (USA).

Devidasrao, S., 2012. Diagnostic verification of atmospheric water cycle predicted by regional mesoscale models and ensemble systems. Ph.D. thesis. Universität Hamburg, Germany.

Doms, G., Schättler, U., Baldauf, M., 2011. A Description of the Nonhydrostatic Regional COSMO Model. Dwd Cosmo V5.4, October.

Drobinski, P., Ducrocq, V., Alpert, P., Anagnostou, E., Béranger, K., Borga, M., Braud, I., Chanzy, A., Davolio, S., Delrieu, G., Estournel, C., Filali Boubrahmi, N., Font, J., Grubišić, V., Gualdi, S., Homar, V., Ivančan-Picek, B., Kottmeier, C., Kotroni, V., Lagouvardos, K., Lionello, P., Llasat, M.C., Ludwig, W., Lutoff, C., Mariotti, A., Richard, E., Romero, R., Rotunno, R., Roussot, O., Ruin, I., Somot, S., Taupier-Letage, I., Tintor, J., Uijlenhoet, R., Wernli, H., 2014. HYMEX: a 10-year multidisciplinary program on the mediterranean water cycle. Bull. Am. Meteorol. Soc. 95 (7) https://doi.org/10.1175/BAMS-D-12-00242.1.

Ducrocq, V., Braud, I., Davolio, S., Ferretti, R., Flamant, C., Jansa, A., Kalthoff, N., Richard, E., Taupier-Letage, I., Ayral, P.A., Belamari, S., Berne, A., Borga, M., Boudevillain, B., Bock, O., Boichard, J.L., Bouin, M.N., Bousquet, O., Bouvier, C., Chiggiato, J., Cimini, D., Corsmeier, U., Coppola, L., Cocquerez, P., Defer, E., Delanoë, J., di Girolamo, P., Doerenbecher, A., Drobinski, P., Dufournet, Y., Fourrié, N., Gourley, J.J., Labatut, L., Lambert, D., le Coz, J., Marzano, F.S., Molinié, G., Montani, A., Nord, G., Nuret, M., Ramage, K., Rison, W., Roussot, O., Said, F., Schwarzenboeck, A., Testor, P., van Baelen, J., Vincendon, B., Aran, M., Tamayo, J., 2014. HyMeX-SOP1: the field campaign dedicated to heavy precipitation and flash flooding in the northwestern Mediterranean, 95. https://doi.org/10.1175/BAMS-D-12-00244.1.

Fosser, G., Khodayar, S., Berg, P., 2015. Benefit of convection permitting climate model simulations in the representation of convective precipitation. Clim. Dyn. 44, 45–60. https://doi.org/10.1007/s00382-014-2242.

Fourrié, N., Nuret, M., Brousseau, P., Caumont, O., Doerenbecher, A., Wattrelot, E., Moll, P., Bénichou, H., Puech, D., Bock, O., Bosser, P., Chazette, P., Flamant, C., Di Girolamo, P., Richard, E., Saïd, F., 2019. The AROME-WMED reanalyses of the first special observation period of the Hydrological cycle in the Mediterranean experiment (HyMeX). Geosci. Model Dev. 12, 2657–2678. https://doi.org/10.5194/gmd-12-2657-2019.

Fourrié, N., Nuret, M., Brousseau, P., Caumont, O., 2021. Data assimilation impact studies with the AROME-WMED reanalysis of the first special observation period of the Hydrological cycle in the Mediterranean Experiment. Nat. Hazards Earth Syst. Sci. 21, 463–480. https://doi.org/10.5194/nhess-21-463-2021.

Hastings, D.A., Dunbar, P.K., 1999. Global Land One-kilometer Base Elevation (Globe). United States Department of Commerce, National Oceanic and Atmospheric Administration, p. 34.

Jacobsen, I., Heise, E., 1982. A new economic method for the computation of the surface temperature in numerical models. Contr. Atmos. Phys. 55, 128–141.

Jiang, Q., Li, W., Wen, J., Qiu, C., Sun, W., Fang, Q., Xu, M., Tan, J., 2018. Accuracy evaluation of two high-resolution satellite-based rainfall products: TRMM 3B42V7 and CMORPH in Shanghai. Water (Switzerland). 10, 40. https://doi.org/10.3390/w10010040.

Joyce, R.J., Janowiak, J.E., Arkin, P.A., Xie, P., 2004. CMORPH: a method that produces global precipitation estimates from passive microwave and infrared data at high spatial and temporal resolution. J. Hydrometeorol. 5 https://doi.org/10.1175/1525-7541(2004)005<0487:CAMTPG>2.0.CO;2.

Kendon, E.J., Ban, N., Roberts, N.M., Fowler, H.J., Roberts, M.J., Chan, S.C., Evans, J.P., Fosser, G., Wilkinson, J.M., 2017. Do convection-permitting regional climate models improve projections of future precipitation change? Bull. Am. Meteorol. Soc. 98 (1) https://doi.org/10.1175/BAMS-D-15-0004.1.

Khodayar, S., Kalthoff, N., Wickert, J., Kottmeier, C., Dorninger, M., 2012. High-resolution representation of the mechanisms responsible for the initiation of isolated thunderstorms over flat and complex terrains: analysis of CSIP and COPS cases.

Meteorog. Atmos. Phys. 119 (3–4), 109–112. https://doi.org/10.1007/s00703-012-0232-6.

Khodayar, S., Kalthoff, N., Kottmeier, C., 2018a. Atmospheric conditions associated with heavy precipitation events in comparison to seasonal means in the western Mediterranean region. Clim. Dyn. 51 https://doi.org/10.1007/s00382-016-3058-y.

Khodayar, S., Czajka, B., Caldas-Alvarez, A., Helgert, S., Flamant, C., di Girolamo, P., Bock, O., Chazette, P., 2018b. Multi-scale observations of atmospheric moisture variability in relation to heavy precipitating systems in the northwestern Mediterranean during HyMeX IOP12. Q. J. R. Meteorol. Soc. 144 https://doi.org/10.1002/qj.3402.

Khodayar, S., Davolio, S., di Girolamo, P., Lebeaupin Brossier, C., Flaounas, E., Fourrie, N., Lee, K.-O., Ricard, D., Vie, B., Bouttier, F., Caldas-Alvarez, A., Ducrocq, V., 2021. Overview towards improved understanding of the mechanisms leading to heavy precipitation in the western Mediterranean: lessons learned from HyMeX. Atmos. Chem. Phys. 21 (22) https://doi.org/10.5194/acp-21-17051-2021.

Lindskog, M., Ridal, M., Thorsteinsson, S., Ning, T., 2017. Data assimilation of GNSS zenith total delays from a Nordic processing Centre. Atmos. Chem. Phys. 17, 13983–13998. https://doi.org/10.5194/acp-17-13983-2017.

Lionello, P., 2012. The climate of the Mediterranean region: from the past to the future. In: The Climate of the Mediterranean Region.

Louis, J.F., 1979. A parametric model of vertical eddy fluxes in the atmosphere. Boundary-Layer Meteorol. 17 (2), 187–202. https://doi.org/10.1007/BF00117978.

Mascitelli, Alessandra, Federico, Stefano, Claudia, Torcasio Rosa, Dietrich, S., 2021. Assimilation of GPS Zenith Total Delay estimates in RAMS NWP model: Impact studies over central Italy. Adv. Space Res. 68 (12), 4783–4793. https://doi.org/10.1016/j.asr.2020.08.031.

Parracho, A.C., Bock, O., Bastin, S., 2018. Global IWV trends and variability in atmospheric reanalyses and GPS observations. Atmos. Chem. Phys. 18, 16213–16237. https://doi.org/10.5194/acp-18-16213-2018.

Poli, P., Moll, P., Rabier, F., Desrozier, G., Chapnik, B., Berre, L., Healy, S.B., Andersson, E., el Guelai, F.Z., 2007. Forecast impact studies of zenith total delay data from European near real-time GPS stations in Météo France 4DVAR. J. Geophys. Res. Atmos. 112 (6) https://doi.org/10.1029/2006JD007430.

Randall, D.A., Wood, R.A., Bony, S., Colman, R., Fichefet, T., Fyfe, J., Kattsov, V., Pitman, A., Shukla, J., Srinivasan, J., Stouffer, R.J., Sumi, A., Taylor, K.E., 2007. Climate models and their evaluation. In: Climate Change 2007: The Physical Science Basis. In Contribution of Working Group I to the Fourth Assessment Report of the Intergovernmental Panel on Climate Change [Solomon, S., D. Qin, M. Manning, Z. Chen, M. Marquis, K.B. Averyt, M.Tignor and H.L. Miller (eds.)] (Vol. 50, Issue 3).

Ricard, D., Ducrocq, V., Auger, L., 2012. A climatology of the mesoscale environment associated with heavily precipitating events over a northwestern Mediterranean area. Appl. Meteorol. 51 (3), 468–488. https://doi.org/10.1175/JAMC-D-11-017.1.

Ritter, B., Geleyn, J.-F., 1992. A comprehensive radiation scheme for numerical weather prediction models with potential applications in climate simulations. Mon. Weather Rev. 120 (2), 303. https://doi.org/10.1175/1520-0493(1992)120<0303:ACRSFN>2.0.CO;2.

Schättler, U., Doms, G., Schraff, C., 2009. A description of the nonhydrostatic COSMO-Model. Part VII: User's guide, report, 147 pp., Consort. for Small-Scale Modell., Dtsch. Wetterdienst, Offenbach, Germany. Available at. http://www.cosmo-model.org/content/model/documentation/core/cosmoUserGuide.pdf.

Schraff, C., Hess, R., 2012. A Description of the Nonhydrostatic Regional COSMO-Model. Part III: Data Assimilation. Deutsche Wetterdienst, P.O. Box 100465, 63004 Offenbach, Germany.

Schraff, C., Tomassini, M., Stephan, K., 2008. Developments at DWD: Integrated water vapour (IWV) from ground-based GPS. COSMO newletter 9, Deutscher Wetterdienst, Frankfurter Strasse 135, 63067 Offenbach, Germany.

Sherwood, S.C., Roca, R., Weckwerth, T.M., Andronova, N.G., 2010. Tropospheric water vapor, convection, and climate. Rev. Geophys. 48 (2) https://doi.org/10.1029/2009RG000301.

Tiedtke, M., 1989. A comprehensive mass flux scheme for cumulus parameterization in large-scale models. Mon. Weather Rev. 117 https://doi.org/10.1175/1520-0493(1989)117<1779:ACMFSF>2.0.CO;2.

Trenberth, K.E., Dai, A., Rasmussen, R.M., Parsons, D.B., 2003. The changing character of precipitation. Bull. Am. Meteorol. Soc. 84 (9), 1205–1218. https://doi.org/10.1175/BAMS-84-9-1205.

Wernli, H., Paulat, M., Hagen, M., Frei, C., 2008. SAL - A novel quality measure for the verification of quantitative precipitation forecasts, 136. https://doi.org/10.1175/2008MWR2415.1.

Zhang, G., Cook, K.H., Vizy, E.K., 2016. The diurnal cycle of warm season rainfall over West Africa. Part I: Observational analysis. J. Clim. 29 (23) https://doi.org/10.1175/JCLI-D-15-0874.1.